Title

HemK2 functions for sufficient protein synthesis and RNA stability through eRF1 methylation during *Drosophila* oogenesis

Running Title

HemK2 functions for translation and RNA stability

Authors

Fengmei Xu[1], Ritsuko Suyama[1], Toshifumi Inada[2], Shinichi Kawaguchi[1]*, and Toshie Kai[1]*

*Corresponding author

E-mail: kawaguchi.shinichi.fbs@osaka-u.ac.jp (KS)

E-mail: kai.toshie.fbs@osaka-u.ac.jp (KT)

Affiliations

[1] Graduate School of Frontier Biosciences, Osaka University, Osaka 565-0871, Japan

[2] Division of RNA and Gene regulation, Institute of Medical Science, The University of Tokyo, Tokyo 108-8639, Japan.

Abstract

HemK2 is a highly conserved methyltransferase spanning from yeast to humans. Despite its conservation, the identification of its genuine substrates has been controversial, and its biological importance in higher organisms remains unclear. In this study, we elucidate the role of HemK2 in the methylation of eukaryotic Release Factor 1 (eRF1), a process essential for female germline development in *Drosophila melanogaster*. Knockdown of *hemK2* in the germline cells (*hemK2*-GLKD) induces apoptosis in these cells, accompanied by a pronounced decrease in both eRF1 methylation and protein synthesis. The overexpression of a methylation-deficient eRF1 variant recapitulates the defects observed in *hemK2*-GLKD, suggesting that eRF1 is a primary methylation target of HemK2. Furthermore, *hemK2*-GLKD leads to significant reduction mRNA levels in germline cell. We demonstrate that these defects in oogenesis and protein synthesis can be partially restored by inhibiting the No-Go Decay pathway. In addition, *hemK2* knockdown is associated with increased disome formation, suggesting that disruptions in eRF1 methylation may provoke ribosomal stalling, which subsequently activates translation-coupled mRNA surveillance mechanisms that degrade actively-translated mRNAs. We propose that HemK2-mediated methylation of eRF1 is critical for ensuring efficient protein production and mRNA stability, which are vital for the generation of high-quality eggs.

Introduction

Post-translational modifications (PTMs), such as methylation, phosphorylation, glycosylation, acetylation, and ubiquitination, are chemical alterations that occur after protein synthesis. PTMs profoundly influence protein function, interaction, stability, and enzymatic activity (Ramazi and Zahiri, 2021; Ryšlavá et al., 2013). Among the over 400 types of PTMs, methylation is one of the most pervasive. Methylation reactions are catalyzed by S-adenosylmethionine-dependent methyltransferases (MTases), which transfer methyl groups to a variety of biomolecules, including proteins, DNA, and RNA, targeting cytosines and adenines (Chen et al., 2013; Dai et al., 2021; Ping et al., 2014; Wang et al., 2016). In the *Drosophila* genome, 127 MTase genes have been annotated, and these MTases have been further classified based on their substrate specificities. Lysine MTases and arginine MTases constitute substantial groups among protein MTases. Prior studies on histone methylation have highlighted the importance of lysine/arginine modifications in transcriptional regulation (Gates et al., 2017; Zhao and Garcia, 2015). In addition to lysine and arginine residues, other amino acid residues such as histidine (Clarke, 2013), aspartic acid (Sprung et al., 2008), asparagine (Klotz et al., 1990), and glutamine (Heurgué-Hamard et al., 2002) are also subject to methylation.

HemK2 is a member of the unclassified protein MTases, distinct due to its broad substrate class. HemK2 has been previously shown to catalyze the methylation of histone H4 lysine 12 (H4K12), DNA N6-adenine (6mA), and eukaryotic translation release factor 1 (eRF1). HemK2-mediated H4K12 methylation is implicated in regulating the proliferation of prostate tumor cells

70 (Metzger et al., 2019), while diminished genomic DNA 6mA levels have been
71 associated with tumorigenesis in cancer patients (Xiao et al., 2018). However,
72 the enzymatic activity of HemK2 towards genomic DNA 6mA remains
73 controversial (Kweon et al., 2019; Ratel et al., 2006; Woodcock et al., 2019).
74 Conversely, HemK2's role as an MTase for eRF1 has been extensively
75 investigated in yeast and mammalian cells. HemK2 (N6AMT1 in humans;
76 YDR140w or Mtq2p in yeast) methylates the glutamine residue within the
77 GGQ motif of eRF1 (Figaro et al., 2008; Heurgué-Hamard et al., 2006; Liu et
78 al., 2010). Depletion of HemK2 in yeast (Mtq2p) resulted in sensitivity to
79 translation-fidelity antibiotics (Polevoda et al., 2006). In mice, HemK2 (also
80 known as N6AMT1) deficiency led to early embryonic lethality and impaired
81 post-implantation development (Liu et al., 2010). Yet, the methylation of these
82 potential substrates by HemK2 under physiological conditions in multicellular
83 organisms is not well defined.
84 *Drosophila* oogenesis serves as an exemplary model for studying the
85 genetic regulation of egg production. The female fly harbors a pair of ovaries,
86 each comprising 18–20 ovarioles, which contain the germarium at the anterior
87 tip, succeeded by sequentially maturing egg chambers (Avilés-Pagán and
88 Orr-Weaver, 2018; Gleason et al., 2018; Rastegari et al., 2020). Each egg
89 chamber encompasses one oocyte and 15 nurse cells that support oocyte
90 growth, surrounded by a monolayer of somatic follicle cells. In nurse cells, the
91 production of mRNAs and proteins for maternal deposition into eggs is critical
92 for proper oogenesis. Consequently, *Drosophila* oogenesis is an energetically
93 demanding process involving cellular proliferation and growth that
94 necessitates extensive protein synthesis (Lasko, 2012).

The role of HemK2 as a methyltransferase (MTase) has been extensively investigated in yeast and mammalian cell cultures. Nonetheless, its function within multicellular organisms, particularly in the reproductive system—characterized by active gene expression and protein synthesis—has not been fully elucidated. In this study, we delineate the role of HemK2 in eRF1 methylation during *Drosophila* oogenesis. Our findings indicate that HemK2 is critical for egg production; knockdown of *hemK2* expression arrested oogenesis at an intermediate stage and induced apoptosis in germline cells. The disruption of *hemK2* expression resulted in a substantial decrease in eRF1 methylation, whereas methylation of DNA 6mA and histone H4 lysine 12 (H4K12) was not significantly affected. Moreover, the lack of eRF1 methylation impaired translation efficiency, which in turn reduced mRNA levels via the No-Go Decay pathway. Collectively, these results highlight the indispensable function of HemK2-mediated eRF1 methylation in promoting effective protein synthesis and mRNA stability, thus modulating gene expression throughout *Drosophila* oogenesis.

Results

Germline knockdown of *hemK2* resulted in female sterility marked by the developmental arrest in the mid-oogenesis

To investigate the role of HemK2, a highly conserved methyltransferase encoded by *CG9960* in *Drosophila melanogaster*, we employed RNA interference to repress its expression. This knockdown was conducted by shRNA targeted to the 3'UTR (BL#40837) using the germline-specific driver *NGT40*; *NosGal4-VP16* (Grieder et al., 2000). In normal development, the oocyte accrues proteins and RNAs from 15 nurse cells through cytoplasmic channels (Fig. 1A, B). Females with germline-specific knockdown of *hemK2* (*hemK2*-GLKD) showed a ~65% decrease in mRNA levels (Fig. 1C, S1A) and exhibited sterility. These *hemK2*-GLKD females contained small ovaries and were incapable of laying eggs (Fig. 1B, D), indicative of developmental arrest at stages 7/8 before the vitellogenic stages. Conversely, *hemK2*-GLKD males, despite a similar reduction in its mRNA level to approximately 25%, did not exhibit notable fertility impairments (Fig. S1F, G).

HemK2 is expressed from a dicistronic transcript which is co-transcribed with the upstream open reading frame, *snapin*, in a single mRNA (Fig. S1A) (Wall et al., 2005). To confirm that the observed defects in *hemK2*-GLKD were due to diminished HemK2 protein expression, individual transgenes coding for N-terminal FLAG-tagged HemK2 or Snapin, lacking the shRNA target sequence, were expressed in the germline following knockdown of the dicistronic mRNA (Fig. 1E; Fig. S1E). Females expressing the *hemK2* transgene alone in their germline exhibited egg laying and hatching rates comparable to controls (Fig. 1D), thus rescuing the sterility defect. In contrast,

137 expression of *snapin* did not restore these defects (Fig. S1D). These results
138 confirm that the sterility observed was specifically due to compromised
139 *hemK2* function resulting from knockdown of the dicistronic transcript,
140 establishing *hemK2*'s vital role in germline cells during oogenesis.

141 To investigate the function of *hemK2* in somatic cells, we knocked
142 down its expression in ovarian somatic cells, including follicle cells, using the
143 somatic driver *traffic jam-Gal4* (*tj-Gal4*). *hemK2*-STKD females became sterile
144 with rudimentary ovaries (Fig. S1B, C). These ovaries often presented with
145 fused egg chambers and disorganized follicle cells (Fig. S1C). Remarkably,
146 the fertility and developmental disruptions were nearly fully rescued by
147 expressing the *hemK2* transgene with *tj-Gal4* (Fig. S1B, C), suggesting that
148 *hemK2* is crucial in both germline and somatic cell functions during
149 oogenesis.

150

151 **Pleiotropic phenotypes in *hemK2*-GLKD ovaries indicate essential roles**
152 **in oogenesis**

153 Ovaries with *hemK2*-GLKD exhibited multiple phenotypic aberrations:
154 hyperplasia of the posterior follicle cells, chromosomal dispersion failure, and
155 extensive apoptosis in germline cells (Fig. 2). All egg chambers in the control
156 females were encapsulated by a monolayer of follicle cells, whereas the
157 majority of egg chambers in *hemK2*-GLKD females demonstrated multi-
158 layered follicle cells in the posterior region (Fig. 2A; 94%). In addition, an
159 increased presence of mitotic cells, marked by phospho-histone H3 (pH3),
160 was observed in the hyperplastic multi-layered follicle cells of *hemK2*-GLKD
161 during stages 7/8 (Fig. 2A).

162 Moreover, nurse cells in *hemK2*-GLKD displayed defective
163 chromosomal dispersion (Fig. 2B). Typically, wild-type nurse cells underwent
164 a distinct polytene chromosome condensation into a '5-blob' structure, which
165 was fully dispersed by stage 6 (Dej and Spradling, 1999). In stark contrast,
166 almost all *hemK2*-GLKD ovarioles contained nurse cell nuclei with
167 chromosomal configurations retained in a blob-like state beyond this stage
168 (Fig. 2B, Fig. S2A; 99%). To investigate the possible causes of this
169 chromosomal defect, we examined the expression levels of genes known to
170 be involved in chromosomal dispersion (Goodrich et al., 2004; Klusza et al.,
171 2013). qRT-PCR analysis showed that the mRNA level of *otu* was significantly
172 reduced in *hemK2*-GLKD ovaries (Fig. 2C), suggesting a correlation between
173 *otu* expression and the chromosomal dispersion defect. The expression of N-
174 terminal FLAG-tagged Otu104 isoform in *hemK2*-GLKD ovaries substantially
175 recovered the dispersion of chromosomes (Fig. S2A), suggesting that *hemK2*
176 supports chromosomal dispersion during oogenesis, partly by ensuring *otu*
177 expression.

178 Additionally, *hemK2*-GLKD led to pronounced degeneration of egg
179 chambers during mid-oogenesis, a process that is typically regulated by
180 germline cell viability in response to physiological and environmental cues
181 (Drummond-Barbosa and Spradling, 2001; McCall, 2004). Immunostaining for
182 p53, an apoptotic inducer, revealed a marked increase in p53 signal in the
183 nurse cell nuclei of most *hemK2*-GLKD ovarioles (Fig. 2D; 93%), suggesting
184 cell death in mid-oogenesis. Consistently, the simultaneous knockdown of *p53*
185 and *hemK2* significantly restored the progression of oogenesis in *hemK2*-
186 GLKD ovaries (Fig. S2B). Furthermore, expression of p35, an inhibitor of

187 caspases DrICE and Dcp-1 (Fuchs and Steller, 2015; Werz et al., 2005) also
188 suppressed the cell death in *hemK2*-GLKD ovaries (Fig. S2B). While females
189 with either *p53* knockdown or ectopic p35 expression in *hemK2*-GLKD did not
190 fully recover egg-laying to control levels, the hatching rates of the resulting
191 eggs were comparable to that of controls (Fig. S2C). Collectively, these data
192 suggest that p53-dependent apoptosis occurs during mid-oogenesis in
193 *hemK2*-GLKD, although the precise initiating mechanisms remain to be
194 determined. Notably, chromosomal dispersion remained impaired in *hemK2*-
195 GLKD ovaries even after cell death suppression (Fig. S2B), indicating that
196 apoptosis and chromosomal dispersion defects are mediated by distinct
197 pathways affected by *hemK2* downregulation.

198

199 **eRF1 methylation by HemK2's catalytic activity is required for oogenesis**
200 Previous studies have identified HemK2 as a methyltransferase acting on
201 three different substrates: DNA N6-adenine (6mA) in human cultured cells
202 (Xiao et al., 2018), histone H4 lysine 12 (H4K12) in A549 lung
203 adenocarcinoma cells (Metzger et al., 2019), and a glutamine residue within
204 the GGQ motif of eRF1 in yeast (Heurgué-Hamard et al., 2005) and human
205 (Figaro et al., 2008). Nonetheless, the genuine substrate and functional role of
206 HemK2 in multicellular organisms have remained elusive. First, we
207 investigated the 6mA modification in genomic germline DNA of *hemK2*-GLKD
208 through immunostaining with an anti-6mA antibody. No alteration in the
209 pattern or signal intensity of 6mA staining was observed in *hemK2*-GLKD
210 germline cells (Fig. S3A), suggesting that HemK2 does not mediate the
211 methylation of genomic N6-adenine in the *Drosophila* germline. Moreover,

212 levels of methylated H4K12 were similar between *hemK2*-GLKD and control
213 ovaries (Fig. S3B), thereby excluding H4K12 as a primary substrate in the
214 *Drosophila* germline.

215 Subsequently, we evaluated the methylation status of endogenous
216 eRF1 in *hemK2*-GLKD ovaries. Due to the ineffectiveness of the anti-methyl-
217 eRF1 antibody in Western blot analyses, we performed eRF1
218 immunoprecipitation followed by immunoblotting with an antibody against N5-
219 methyl-glutamine (methyl-Q). The eRF1 methylation in *hemK2*-GLKD ovaries
220 was significantly reduced to 35% of control, likely reflecting the contribution
221 from unaffected somatic cells (Fig. 3A). Immunostaining with the anti-methyl-
222 eRF1 antibody showed a substantial reduction of eRF1 methylation
223 specifically in germline cells of *hemK2*-GLKD ovaries, while the expression
224 level of eRF1 remained consistent across cell types (Fig. 3B). This finding
225 was corroborated by the immunoprecipitation of FLAG-tagged eRF1
226 expressed in the germline, which exhibited minimal methylation in *hemK2*-
227 GLKD ovaries compared to control (Fig. 3C), confirming the role of *Drosophila*
228 HemK2 in eRF1 methylation. It is well documented that a glutamine residue
229 within the GGQ motif of eRF1, crucial for peptide release, is consistently
230 methylated by HemK2 across various species (Dinçbas-Renqvist et al., 2000;
231 Figaro et al., 2008; Gao et al., 2020; Kusevic et al., 2016; Svidritskiy and
232 Korostelev, 2018). To determine if the GGQ motif of eRF1 is the methylation
233 target in *Drosophila*, we mutated the corresponding glutamine (Q185) to
234 alanine (eRF1 Q185A) and examined their methylation in S2 cells (Fig. 3D).
235 Consistent with observations in other systems, methylation of the eRF1
236 Q185A mutant was nearly undetectable, irrespective of *hemK2* knockdown,

237 indicating that this mutation disrupts eRF1 methylation (Fig. 3D). Collectively,
238 these results suggest that Q185 is the predominant methylation site of eRF1
239 by *Drosophila* HemK2.

240 The abovementioned rescue experiments validated HemK2's
241 indispensable role *in vivo* for egg development (Fig. 1 and Fig. S1). We
242 proceeded to evaluate the significance of amino acid residues critical for
243 HemK2's methyltransferase activity during oogenesis. The NPPY motif of
244 HemK2, highly conserved and recognized as a substrate-binding pocket, is
245 vital for its methylation function in human cell lines (Fig. 4A) (Gao et al., 2020;
246 Metzger et al., 2019). It has been reported that mutations in residues proximal
247 to the substrate, specifically Asn122 and Tyr125 within the NPPY motif of
248 human HemK2, abolish its catalytic activity for eRF1 methylation *in vitro* (Fig.
249 4B) (Metzger et al., 2019). Correspondingly, we introduced mutations at
250 analogous positions in *Drosophila* HemK2, Asn116 and Tyr119, substituting
251 them with alanine (N116A and Y119A, respectively), and expressed these
252 mutants in the germline of *hemK2*-GLKD ovaries (Fig. 4C; Fig. S4A). The
253 Y119A mutant did not recover the observed defects, such as egg chamber
254 degeneration, egg laying and hatching rate, however, the N116A mutant
255 restored these parameters to levels comparable to the control (Fig. 4C, D).
256 These findings suggest that Tyr119, as opposed to Asn116, is critical for
257 HemK2's function within *Drosophila* germline cells.

258 Furthermore, we investigated HemK2's activity in catalyzing the
259 methylation of the glutamine residue within the GGQ motif of eRF1 in S2 cells.
260 After co-transfecting each FLAG-tagged HemK2 variant with Myc-tagged
261 eRF1 into S2 cells and knocking down endogenous *hemK2*, we assessed

262 eRF1 methylation (Fig. 4E). Immunoprecipitation of Myc-eRF1 followed by
263 immunoblotting with an anti-methyl-Q antibody showed significant reduction in
264 eRF1 methylation upon endogenous *hemK2* knockdown. This reduction was
265 rescued by expressing wildtype HemK2 and the N116A mutant, but not by the
266 Y119A mutant (Fig. 4E). This demonstrates that Tyr119, but not Asn116, is
267 indispensable for the methylation of eRF1 at the 185th glutamine by
268 *Drosophila* HemK2.

269 Additionally, given that HemK1, a paralog of HemK2 with a conserved
270 NPPY motif and 42% sequence homology, is known to methylate the
271 glutamine in the GGQ motif of mitochondrial release factors in human cells
272 (Fang et al., 2022; Ishizawa et al., 2008), we sought to determine the
273 specificity of cytosolic eRF1 methylation by HemK2. In S2 cells, where *hemK2*
274 knockdown reduced eRF1 methylation, expression of HemK2, but not
275 HemK1, rescued the methylation levels, signifying that cytosolic eRF1
276 methylation is an exclusive function of HemK2 (Fig. S4B).

277

278 **HemK2-mediated eRF1 methylation is required for the efficient**
279 **translation and mRNA stability**

280 We investigated the role of eRF1 methylation in oogenesis by knocking down
281 *eRF1* expression in germline cells. *eRF1* germline knockdown (*eRF1*-GLKD)
282 led to rudimentary ovaries that failed to produce eggs, a phenotype more
283 severe than that of *hemK2*-GLKD (Fig. 1B, 5A, B). Immunostaining with Vasa
284 (Vas), a DEAD box RNA helicase and germline marker, indicated agametic
285 germaria with a stark reduction in germline cells in *eRF1*-GLKD ovaries (Fig.

286 5C). The defects in *eRF1*-GLKD were successfully rescued by expressing
287 FLAG-tagged wildtype eRF1, but not with the methylation-deficient Q185A
288 mutant in germline cells (Fig. 5B, C). This highlights the critical role of the
289 185th glutamine residue, and likely its methylation, in germline cell viability and
290 oogenesis progression. The less severe phenotype in *hemK2*-GLKD could
291 result from incomplete disruption of eRF1 methylation, potentially due to
292 residual *hemK2* expression or compensation by other methyltransferase(s).

293 Moreover, expressing FLAG-eRF1 Q185A mutant in germline cells of
294 wildtype ovaries disrupted egg production (Fig. 5D). This expression led to
295 developmental arrest at mid-oogenesis, with defects in chromosome
296 dispersion and extensive apoptosis, mirroring the *hemK2*-GLKD phenotype
297 (Fig. 5D; Fig. S5A, B). Over 80% of ovarioles expressing eRF1 Q185A
298 exhibited p53-positive egg chambers (Fig. S5C). Therefore, the expression of
299 eRF1 Q185A effectively recapitulates the *hemK2*-GLKD phenotype,
300 supporting that the absence of eRF1 methylation primarily causes the
301 observed defects.

302 Given that eRF1 GGQ motif methylation is essential for nascent
303 peptide release and translational termination efficiency, and that its
304 perturbation could lead to translational deficits by hindering ribosome
305 recycling, we assessed translation activity in *hemK2*-GLKD ovaries using an
306 HPG incorporation assay *ex vivo*. HPG, a methionine analog with an alkyne
307 group, can be incorporated into newly synthesized proteins and is visualized
308 through a 'Click reaction' with a fluorescent dye (Shen et al., 2021). A notable
309 decrease in HPG signal in cytoplasm of germline cell was observed in
310 *hemK2*-GLKD ovaries (Fig. 5E), indicating a requirement for eRF1

311 methylation in maintaining translation efficiency. This translational reduction in
312 *hemK2*-GLKD was completely restored by expressing either wildtype HemK2
313 or the N116A mutant, but not by the Y119A mutant (Fig. 5E). Similarly,
314 germline expression of the methylation-deficient eRF1 Q185A mutant
315 abrogated translation activity (Fig. S5D). Collectively, these results
316 underscore the necessity of HemK2-mediated eRF1 methylation for efficient
317 translation in the *Drosophila* ovary.

318 To elucidate the molecular deficiencies resulting from *hemK2*-GLKD
319 and eRF1 dysfunction, we conducted ovarian mRNA-seq analysis using next-
320 generation sequencing technology. Late egg chambers in control ovaries
321 were selectively removed to minimize developmental discrepancies between
322 *hemK2*-GLKD and control samples. Aligning with our RT-PCR data (Fig. 1C
323 and Fig. 2C), mRNA-seq confirmed the marked downregulation of *hemK2*
324 (log2FC=-1.27) and *otu* (log2FC=-1.45) (Supplementary Table S4).
325 Additionally, we identified 478 upregulated and 325 downregulated genes
326 ($\log_2$FC < -1 or > 1; q-val < 0.01). Gene Ontology (GO) term analysis (Thomas
327 et al., 2022) of differentially expressed genes indicated a significant
328 downregulation in genes associated with female reproductive processes, such
329 as female gamete generation, oogenesis, and germ cell development (Fig.
330 6A), while genes unrelated to oogenesis were comparatively upregulated (Fig.
331 6B).

332 To further dissect the gene expression changes following germline
333 knockdown of *hemK2*, we referenced a previous study detailing gene
334 expression across different ovarian cell types from single-cell mRNA
335 analyses; many different cell types were distinguished based on gene

336 expression patterns. Focusing on genes expressed in one germline and five
337 somatic cell types representing early to mid-oogenesis, we observed a
338 significant downregulation (average $\log_2$FC = -0.55) in *hemK2*-GLKD for
339 genes enriched in germline 2 cell type (N=154), which are expressed from
340 germarium region 2 onward (Fig. 6C, D) (Jevitt et al., 2020). In contrast,
341 genes associated with the five somatic cell types did not show notable
342 changes (Fig. 6D; Fig. S6A-E), suggesting that *hemK2*-GLKD specifically
343 downregulates mRNAs in germline cells.

344 Previous research indicates that eRF1 methylation at the GGQ motif
345 substantially enhances the release of nascent peptides, accelerating
346 translation termination by 10 to 100-fold (Pierson et al., 2016). We
347 hypothesize that impaired methylation on eRF1 could decrease the peptide
348 release rate, leading to ribosome stalling at stop codons of actively translated
349 mRNAs. Such stalling is known to activate mRNA surveillance process,
350 targeting mRNAs with engaged ribosomes for degradation via the No-Go
351 Decay (NGD) pathway (Brandman and Hegde, 2016; Doma and Parker,
352 2006; Ikeuchi et al., 2019; Simms et al., 2017; Tomomatsu et al., 2023). To
353 investigate this hypothesis, we analyzed ribosome stalling in *hemK2*-GLKD by
354 performing a sucrose gradient sedimentation assay with ovarian lysates. The
355 lysates, treated with emetine to halt translation and RNase A to digest
356 unprotected mRNA regions, revealed a predominance of monosomes and a
357 negligible disome presence in the control, indicative of minimal ribosome
358 stalling and collision (Fig. 6E). However, in *hemK2*-GLKD, disome levels
359 increased approximately 2.1-fold (Fig. 6F, *hemK2*-GLKD), suggesting that

360 ineffective nascent polypeptide release due to unmethylated eRF1 leads to
361 ribosome collision.

362

363 **Blockage of the No-Go Decay pathway restores mRNA destabilization**
364 **and mid-oogenesis arrest in *hemK2*-GLKD ovaries**

365 To ascertain if the No-Go Decay (NGD) pathway was responsible for the
366 pronounced defects observed in *hemK2*-GLKD, we conducted a simultaneous
367 knockdown of the mRNA surveillance pathway components along with *hemK2*
368 in germline cells (Fig. 7 and Fig. S7A). In the double-germline knockdown
369 (DGKD) of *hemK2* and *ski8*—a component of the Ski complex that
370 collaborates with the exosome and facilitates 3' to 5' mRNA degradation
371 (Zinoviev et al., 2020)—, developmental impairments associated with *hemK2*-
372 GLKD were partially restored (Fig. 7A). Females from the *ski8*-*hemK2* DGKD
373 had more advanced stages of egg chambers and laid a comparable number
374 of eggs to controls, though their hatching rate was reduced to 40% of the
375 control (Fig. 7A, B). Considering the Ski complex's role in general RNA decay,
376 we further investigated additional NGD factors, such as *pelota* (*pelo*), which is
377 crucial for dissociating stalled ribosomes and promoting RNA decay within the
378 NGD and No-Stop Decay (NSD) pathways (Becker et al., 2011; Jamar et al.,
379 2017; Kobayashi et al., 2010; Tsuboi et al., 2012). Remarkably, *pelo*-*hemK2*
380 DGKD females exhibited a similar phenotype to that of the *ski8*-*hemK2*
381 DGKD, with advanced egg chamber development and a 60% hatching rate,
382 comparable to the number of eggs laid (Fig. 7A, B). Furthermore, the mid-
383 oogenesis arrest induced by expressing the dominant-negative eRF1 Q185A

384 mutant was also partly rescued by the germline knockdown of either *ski8* or
385 *pelo* (Fig. S7B), reinforcing the notion that the eRF1 methylation defect
386 triggers mRNA surveillance mechanisms.

387 Investigating the role of the NGD pathway in the defects seen in
388 *hemK2*-GLKD ovaries, we assessed another putative NGD component, *nonu-*
389 *1*/*cue2*, an endonuclease identified in *C. elegans* and *S. cerevisiae* that
390 cleaves mRNA near a stalled ribosome during translation (D'Orazio et al.,
391 2019; Glover et al., 2020) (Fig. S7C). Contrasting with the partial rescue
392 observed with *ski8* and *pelo* knockdowns, the simultaneous germline
393 knockdown of *CG7139*, encoding the *Drosophila* ortholog of *nonu-1*/*cue2*, and
394 *hemK2* did not ameliorate the observed phenotypic defects (Fig. 7A, B; Fig.
395 S7A). This indicates that *CG7139* may not be an essential component of the
396 NGD pathway in *Drosophila*, or it may act redundantly with other
397 endonucleases in the translation-coupled mRNA surveillance mechanism
398 compromised by *hemK2* knockdown. Further analysis revealed that a dual
399 germline knockdown of *hemK2* and *upf3*, a factor in Nonsense-Mediated
400 Decay (NMD) (Tan et al., 2022), did not reverse the phenotypic abnormalities
401 in *hemK2*-GLKD ovaries (Fig. 7A, B), emphasizing a specific role of NGD in
402 mediating mRNA degradation. The efficiency of the knockdown for each
403 component was verified by qRT-PCR (Fig. S7A; ranging from 10 to 40%
404 relative to control), accounting for the contribution of non-knockdown somatic
405 cells to the total ovarian RNA, confirming a significant reduction in expression
406 levels. Consistent with their roles in rescuing developmental morphology, the
407 HPG incorporation assay demonstrated that knockdown of *ski8* or *pelo*, but
408 not *CG7139* or *upf3*, in *hemK2*-GLKD ovaries partially restored translational

activity (Fig. 7C, D). These results support the hypothesis that disrupted eRF1 methylation in *hemK2*-GLKD leads to compromised translation termination and ribosome stalling, specifically triggering mRNA degradation via the NGD pathway.

In alignment with the recovery of oogenesis defects in *hemK2*-GLKD, the expression levels of downregulated protein-coding RNAs were restored by the additional germline knockdown of either *ski8* or *pelo* (Fig. 7E, Fig. S6F, G), further validating the specific activation of NGD upon *hemK2*-GLKD. The concurrent germline knockdown of *ski8* or *pelo* with *hemK2* also reinstated general protein synthesis, despite the observation of ribosome stalling to a similar degree as in the single *hemK2* knockdown (Fig. 6E, F). These findings suggest that when mRNAs are not eliminated by NGD, translation re-initiation may occur, enabling protein synthesis and partially recovering egg maturation (Fig. 7A, B). Overall, our results indicate that perturbations in eRF1 methylation due to *hemK2*-GLKD result in the inefficient release of synthesized peptides and the activation of the NGD pathway, likely due to ribosome stalling.

427 **Discussion**

428 The reduction of *hemK2* expression led to female sterility, marked by a
429 significant interruption of oogenesis in both germline and somatic cells of the
430 ovary, culminating in developmental arrest during the mid-stages (Fig. 1; Fig.
431 S1). Notably, *hemK2*-GLKD ovaries exhibited morphological aberrations, such
432 as follicle cell hyperplasia and chromosomal dispersion failure (Fig. 2A, B). It
433 has been previously reported that the expression of the Delta ligand in
434 germline cells activates Notch-Delta signaling pathway, which prompts the
435 transition from the mitotic cell cycle to the endocycle in follicle cells (Deng et
436 al., 2001; Schaeffer et al., 2004; St. Johnston, 2001). The hyperplasia
437 observed in the posterior follicle cells of *hemK2*-GLKD ovaries might be due
438 to diminished Delta ligand expression in germline cells, leading to an
439 extended period of mitotic division in follicle cells beyond the stage 6.

440 In egg chambers of stage 6 and beyond, *hemK2*-GLKD ovarioles
441 predominantly contained nurse cell nuclei with unspread chromosomes (Fig.
442 2B; Fig. S2A). Inhibition of cell death in *hemK2*-GLKD ovaries significantly
443 improved egg chamber formation, yet the chromosomal dispersion defect
444 persisted (Fig. S2B). These findings imply that germline cell death in *hemK2*-
445 GLKD is not caused by the failure of chromosomal dispersion but likely due to
446 ribosome stalling, which is a consequence of eRF1 methylation disturbance
447 (Wu et al., 2020). It has been reported that ribosome collisions can initiate two
448 distinct stress response pathways: a transient collision may trigger a GCN2-

449 mediated pathway promoting cell survival, while more severe collisions could
450 lead to the activation of MAPKK, inducing apoptosis in human cell lines (Wu
451 et al., 2020). Our data suggest that perturbation of methylation due to *hemK2*-
452 knockdown results in ribosome stalling and subsequent collisions, triggering
453 apoptosis in the translationally active environment of *Drosophila* ovaries.

454 Although HemK2 in yeast and mammalian cells has been shown to
455 mediate methylation of DNA 6mA, histone H4K12, and eRF1 (Figaro et al.,
456 2008; Metzger et al., 2019; Xiao et al., 2018), our findings indicate that in
457 *Drosophila*, HemK2 does not affect the methylation of DNA 6mA or histone
458 H4K12 (Fig. S3A, B). Instead, *hemK2* knockdown led to a substantial
459 decrease in eRF1 methylation (Fig. 3A-C), underscoring eRF1 as the specific
460 substrate for *Drosophila* HemK2. Notably, Tyr119, but not Asn116, is
461 essential for HemK2's methyltransferase activity, which is pivotal for
462 oogenesis and eRF1 methylation in *Drosophila* (Fig. 4C-E). This contrasts
463 with the necessity of both corresponding residues in human HemK2 for eRF1
464 methylation in vitro (Metzger et al., 2019). However, recent structural analyses
465 of human HemK2 revealed that the Asn122 side chain does not interact with
466 the methylated glutamine within the substrate binding pocket (Gao et al.,
467 2020), aligning with the dispensability of Asn116 in *Drosophila* HemK2's
468 methyltransferase activity.

469 Murine HemK2 substrate specificity studies using a peptide array have
470 delineated a putative consensus motif: G-Q-[SRYKLGAMTC]-

471 [ARFGLWYCSQKH]-[LARCQFYT]-R, where square brackets indicate any of
472 the residues listed therein (Kusevic et al., 2016). Employing this motif, we
473 have identified several *Drosophila* proteins, including CG17841, Spargel,
474 Chd1, Ythdc1, and eRF1, as potential HemK2 substrates. These candidates
475 may undergo methylation by HemK2 under certain conditions. However, the
476 phenotypes associated with the overexpression of the methylation-deficient
477 eRF1 Q185A mutant mirrored those observed in *hemK2*-GLKD (Fig. 5D),
478 proposing that in the context of *Drosophila* germline cells, eRF1 is the primary
479 substrate for HemK2.

480 Consistent with previous reports, methylation of the conserved GGQ motif
481 within release factors has been shown to significantly enhance nascent
482 peptide release, accelerating the termination rate of protein synthesis by 10 to
483 100-fold (Pierson et al., 2016). Corroborating this, our study found that
484 perturbation of eRF1 methylation by *hemK2*-GLKD led to a marked decrease
485 in translation efficiency (Fig. 5E). Notably, the reduced protein synthesis,
486 alongside the defects in oogenesis and the downregulation of mRNAs, were
487 substantially rescued by inhibiting general RNA degradation and NGD
488 pathway, while NMD blockade did not yield similar results (Fig. 7A-D). These
489 findings imply that the ribosome, even when associated with unmethylated
490 eRF1, can synthesize minimal yet essential polypeptides, provided that the
491 mRNAs are available for translation.

492 Our findings support the role of HemK2 as an authentic protein

493 methyltransferase in *Drosophila*, crucially involved in modulating eRF1 activity
494 via glutamine methylation, a modification vital for appropriate germline
495 development. Germline nurse cells efficiently produce proteins and mRNAs
496 destined for transfer to the oocyte, necessitating stringent regulation of
497 resource-intensive protein synthesis. Nonetheless, the specific regulatory
498 mechanisms governing eRF1 methylation by HemK2 remain elusive and
499 warrant additional exploration. It is plausible that this mechanism serves to
500 optimize egg production under favorable physiological conditions, while
501 downregulating it when conditions are less than ideal.
502

503 **Materials and Methods**

504 **Fly stocks and cultures**

505 All *Drosophila* stocks and crosses were raised at room temperature or at 25°C
506 on standard food (5% (w/v) dry yeast, 5% (w/v) corn flower, 2% (w/v) rice
507 bran, 10% (w/v) glucose, 0.7% (w/v) agar, 0.2% (v/v) propionic acid, and
508 0.05% (w/v) *p*-hydroxy butyl benzoic acid). For RNAi-mediated knockdown
509 experiments, the following transgenic RNAi Project (TRiP) lines from the
510 Bloomington Drosophila Stock Center (BDSC, USA), were utilized: *hemK2*
511 (HMS02003, #40837), *eRF1* (HMS05812, #67900), *upf3* (HMJ22158,
512 #58181), *cue2* (HMS02721, #44007), *ski8* (HMC04664, #57377), and *p53*
513 (HMS02286, #41720). The attP40 (#25709) and attP2 (#25710) lines were
514 employed for transgene injections. The following drivers were used to express
515 transgenes or shRNAs: *NGT40* and *nosGal4-VP16* (Grieder et al., 2000),
516 *Matα-tub-Gal4* (#7063), and *traffic jam-Gal4* (Drosophila Genetic Resource
517 Center, Japan, #104055) (Hayashi et al., 2002). The UASp-P35 transgenic
518 line was generously provided by Dr. Bergmann (Werz et al., 2005). Controls
519 for each experiment were either the *y w* strain or the corresponding
520 heterozygous line.

521

522 **Generation of transgenic fly lines**

523 The transgenic fly lines generated were as follows: FLAG-HemK2 wildtype at
524 attP2, FLAG-HemK2 N116A at attP2, FLAG-HemK2 Y119A at attP2, FLAG-
525 Snapin at attP2, FLAG-eRF1 wildtype at attP2, FLAG-eRF1 Q185A at attP2,
526 and FLAG-Otu104 at attP2. In each instance, the coding sequence or its mutant

527 variant was amplified by PCR, utilizing *y w* genomic DNA or cDNA synthesized
528 from *y w* ovarian RNA as templates. A triple FLAG tag sequence was appended
529 to the N-terminal region of the amplification products. The purified PCR
530 fragments were subsequently cloned into the *Xba*I-linearized pUASp-K10-attB
531 vector (Koch et al., 2009) via In-Fusion reaction (#639648, Takara Bio, Japan).
532 Plasmids confirmed to be correct were injected into embryos of nos-
533 phiC31;;P{CaryP} attP2 (#25710) following standard protocols.

534 The *hemK2* TRiP construct at attP2 and *pelo* TRiP constructs at attP2
535 and attP40 sites, were also created. These TRiP constructs were produced by
536 ligating annealed oligonucleotides (TRiP-Fw/Rv) into the *Nhe*I- and *Eco*RI-
537 linearized pWalium22 vector (Perkins et al., 2015). UASp and Walium22
538 plasmids were then injected into embryos of nos-phiC31; P{CaryP}attP40
539 (#25709) or nos-phiC31;;P{CaryP} attP2 (#25710). The sequences of the
540 oligonucleotides used for annealing are provided in Supplementary Table S1.

541

542 **Fluorescent immunostaining**

543 Immunostaining was performed as previously described (Lim et al., 2022).
544 Ovaries were dissected and slightly teased apart in phosphate-buffered saline
545 (PBS), then fixed with 5.3% (v/v) paraformaldehyde (PFA, Electron Microscopy
546 Sciences, USA) in PBS for 10 min at room temperature. The fixed ovaries were
547 washed for 30 min with several changes of PBX (PBS containing 0.2% (v/v)
548 Triton X-100). This was followed by a blocking step involving incubation in PBX
549 containing 4% (w/v) bovine serum albumin (BSA) for a minimum of 30 min.
550 Ovaries were incubated with primary antibodies diluted in PBX containing 0.4%

551 (w/v) BSA overnight at 4°C, then washed for 1 h with several changes of PBX.
552 Secondary antibodies were applied for over 2 hours at room temperature;
553 following this, ovaries were washed for 1 h with PBX and stained with 1 μg/ml
554 of 4′,6-diamidino-2-phenylindole (DAPI) (SIGMA, USA) for 10 min in PBX. After
555 a final rinse with PBS, the ovaries were mounted onto slides using Fluoro-
556 KEEPER Antifade (Nacalai Tesque, Japan)

557 The following primary antibodies were used in the indicated dilution;
558 mouse anti-FLAG (SIGMA [M2], F1804, 1:200), guinea pig anti-Vas (1:2,000)
559 (Patil and Kai, 2010), rabbit anti-pH3 (Millipore, 06-570, 1:250), mouse anti-p53
560 (DSHB [25F4], 1:100), rabbit anti-Fibrillarin (Abcam, ab5821, 1:200), rabbit
561 anti-DNA 6mA (Synaptic Systems, 202003, 1:1,000), rabbit anti-eRF1 (SIGMA,
562 E8156, 1:200), and rabbit anti-methyl-eRF1 (1:100) (Lacoux et al., 2020).
563 Secondary antibodies were Alexa Fluor 488-, 555- conjugated goat antibodies
564 against rabbit, mouse, and guinea pig IgG (Invitrogen, A11029, A11034,
565 A11073, A21424, A21429, A21435) at a 1:200 dilution in PBX containing 0.4%
566 (w/v) BSA. Ovarian images were captured using a Zeiss LSM 900 confocal
567 microscope and processed with Zen (Zeiss) and Fiji (Schindelin et al., 2012)
568 software.

569

570 **Protein synthesis assay**

571 Protein synthesis was assessed using the Click-iT® L-homopropargylglycine
572 (HPG) Alexa Fluor 488 Protein Synthesis Assay Kit (Molecular Probes, USA),
573 which measures newly synthesized proteins through quantification of the
574 fluorescent HPG signal. Freshly dissected ovaries were incubated in 1 mM

575 HPG in PBS for 30 min and then fixed with 5.3% PFA in PBS for 10 min.
576 Subsequently, the ovaries were permeabilized by washing three times in PBX
577 for 30 minutes: the first wash utilized 3% BSA in PBX, followed by two additional
578 washes in PBX alone. The ovaries were then incubated with a freshly prepared
579 Click-iT® reaction cocktail for 30 min. After washing with Click-iT® reaction
580 rinse buffer, ovaries were stained with HCS NuclearMask™ Blue Stain working
581 solution (1:2,000 in PBX) for 30 min as per the manufacturer's instructions.
582 Subsequent immunostaining with antibodies and image acquisition were
583 performed as described above.

584

585 **Quantification of HPG signal intensity for translation activity**

586 Fluorescence intensity of HPG signals in nurse cells of egg chambers (between
587 stages 3 to 8), was quantified to assess translation activity. Identically sized
588 small squares were selected within the cytosolic areas, avoiding the nucleus.
589 The fluorescence intensity for each square was measured after background
590 subtraction, with the background defined as a blank region lacking any cells or
591 signals. For each egg chamber, 2 to 5 of these squares were analyzed. The
592 average fluorescence intensity across all squares within an image was
593 calculated to represent the translation activity. This process was repeated for a
594 total of 5 images per genotype. Image processing and analysis were conducted
595 using Fiji software.

596

597 **Immunoprecipitation and Western blotting**

598 For immunoprecipitation, 100 ovaries were dissected in cold PBS and

599 homogenized using a pestle in PBS with 0.1% (v/v) Tween-20 (PBST),
600 supplemented with a protease inhibitor cocktail (PIC, 11873580001, Roche,
601 Switzerland). After centrifugation at 15,000 xg for 10 min at 4°C, the
602 supernatant was collected. Protein G magnetic beads (TAMAGAWA SEIKI,
603 TAS8848N1173) were pre-incubated with anti-FLAG antibody (SIGMA [M2],
604 F1804) for more than 1 h at 4°C with gentle rotation before adding lysate. The
605 antibody-conjugated beads were washed twice with cold PBST and then
606 incubated with the lysate for 3-4 hours at 4°C. The proteins were washed three
607 times with cold PBST and eluted from the beads in 50 μl of sample buffer at
608 95°C for 5 min.

609 For Western blotting, ovary lysates or immunoprecipitates were
610 separated by SDS-PAGE and transferred onto a 0.45 μm Clear Trans® PVDF
611 membrane (Wako, Japan). The membrane was blocked in PBST with 3% (w/v)
612 skim milk (Nacalai Tesque, Japan) and incubated with primary antibodies
613 diluted in HIKARI signal enhancer (Nacalai Tesque). The primary antibodies
614 used included rabbit anti-eRF1 (SIGMA, E8156, 1:1,000), rabbit anti-methyl-Q
615 (Millipore, ABS2185, 1:1,000), mouse anti-FLAG (SIGMA [M2], F1804, 1:1,000),
616 mouse anti-c-Myc (Wako [9E10], 017-21871, 1:1,000), mouse anti-histone H4
617 (MAB Institute, 388-09171, 1:2,000), rabbit anti-H4K12met (PTM BIO, PTM-
618 685RM, 1:2,000), mouse anti-Tubulin (Santa Cruz [DM1A], sc-32293, 1:3,000),
619 rabbit anti-HA (Cell Signaling Technology [C29F4], 3724, 1:1,000). Horseradish
620 peroxidase (HRP)-conjugated secondary antibodies used were goat anti-rabbit
621 IgG or anti-mouse IgG (Bio-Rad, 170-6515 or 170-6516, 1:3,000). To prevent
622 signal overlap from IgG heavy chain with eRF1, VeriBlot-HRP (Abcam,
623 ab131366, 1:1,000) was used in Western blot analysis for immunoprecipitation

624 of endogenous eRF1 or FLAG-eRF1. Chemiluminescent signals were detected
625 using Chemi-Lumi One (Nacalai Tesque, 07880-70) and imaged by the
626 ChemiDoc™ Touch MP system (Bio-Rad). Band intensities were quantified
627 using Image Lab software (Bio-Rad) from independent experiments.

628

629 **Quantitative RT-PCR**

630 Total RNA was extracted from ovaries using TRIzol LS Reagent (Invitrogen)
631 strictly according to the manufacturer's instructions. The purified RNA (1 μg)
632 was then treated with DNase I (Invitrogen) to remove any genomic DNA
633 contamination. This was followed by inactivation of the DNase I with EDTA.
634 Reverse transcription to synthesize cDNA was conducted using the Superscript
635 III First-Strand Synthesis System (Invitrogen), as per the manufacturer's
636 protocol. Quantitative PCR (qPCR) was performed using the KAPA SYBR Fast
637 qPCR Master Mix (KAPA Biosystems) on the StepOnePlus Real-Time PCR
638 System (Applied Biosystems). Relative expression levels were normalized to
639 those of the reference gene *rp49* across three biological replicates. The primer
640 sequences used to determine gene expression levels are listed in
641 Supplementary Table S2.

642

643 **S2 cell experiments**

644 *Drosophila* S2 cells were maintained at 28°C in Schneider's medium,
645 supplemented with 10% (v/v) fetal bovine serum (FBS) and antibiotics (penicillin
646 and streptomycin). Knockdown of endogenous *hemK2* was achieved using
647 double-stranded RNA (dsRNA) targeting a 186 bp region from the ATG start

648 codon of the *snapin* gene (refer to Fig. S1). The dsRNA was synthesized using
649 the AmpliScribe T7 High Yield Transcription Kit (Lucigen, USA). Primer
650 sequences for the PCR amplification are provided in Supplementary Table S3.

651 For transfection, plasmids employed were Myc-HemK2 wildtype, Myc-
652 HemK2 N116A, Myc-HemK2 Y119A, FLAG-eRF1 wildtype, FLAG-eRF1
653 Q185A, and Myc-HemK1. These constructs were prepared using the Gateway
654 Cloning System (Life Technologies) and transfected into S2 cells using HilyMax
655 (Dojindo Molecular Technologies, Inc., Japan) according to the manufacturer's
656 protocol.

657

658 **Fertility test**

659 To assess female fertility, *y w* males were paired with three eclosed females of
660 each genotype. Mating was allowed to proceed for several days in vials
661 containing standard food. Subsequently, the flies were transferred to apple juice
662 plates supplemented with a small quantity of moist yeast paste. The total count
663 of eggs laid by the mated females was recorded. After a 24-hour period, the
664 number of unhatched eggs was tallied to calculate the hatching rates. For the
665 evaluation of male fertility in the *hemK2*-GLKD line, three *y w* virgin females
666 were mated with *hemK2*-GLKD males over an extended duration. The fertility
667 metrics for the males were documented in a manner analogous to that
668 described above. Each fertility assessment was replicated across three
669 independent biological samples.

670

671 **mRNA-seq analyses**

672 Total RNA for each genotype was extracted in duplicate from dissected ovaries
673 using TRIzol LS (Invitrogen) following the manufacturer's instructions. Because
674 *hemK2* knockdown ovaries did not contain later stages, regions post-mid
675 oogenesis were excised from *hemK2* knockdown ovaries prior to RNA
676 extraction. Poly(A)-tailed RNAs were enriched and purified using oligo-dT
677 beads from the NEBNext Poly(A) mRNA Magnetic Isolation Module (New
678 England Biolabs, USA). These samples then underwent fragmentation, reverse
679 transcription, adapter ligation, and PCR amplification to prepare cDNA libraries
680 using the NEBNext Ultra II Directional RNA Library Prep Kit (New England
681 Biolabs, USA). Library preparation and next-generation sequencing were
682 outsourced to Rhelixa Inc. (Japan), yielding approximately 13 million paired-
683 end sequences per sample. The fastp program (Chen et al., 2018) was utilized
684 to remove the sequences of low quality and adapter. Alignment to the
685 *Drosophila melanogaster* reference genome (dm6) was conducted using the
686 STAR program (Dobin et al., 2013). Read quantification at the gene level was
687 performed with featureCounts (Liao et al., 2014). Differential expression
688 analysis was executed via DESeq2 (Love et al., 2014), selecting upregulated
689 ($\log_2$FoldChange > 1, p-adj < 0.01) and downregulated ($\log_2$FoldChange < -1,
690 p-adj < 0.01) genes for further GO term enrichment analysis using PANTHER
691 (Thomas et al., 2022).

692

693 **Monosome/Disome profiling**

694 Ovaries were dissected in polysome lysis buffer (20 mM Tris-Cl, pH 7.5, 5 mM
695 $MgCl_2$, 100 mM NaCl) with the addition of 0.1% NP-40, 200 μg/ml emetine

696 (Sigma, E2375), and PIC. Dissected ovaries were snap frozen in liquid nitrogen
697 and stored at -80ºC. Homogenization was performed with a plastic pestle in 500
698 µl of polysome lysis buffer supplemented with 0.1% CHAPS (Nacalai Tesque,
699 Japan), emetine, and PIC. The homogenate was subjected to sequential
700 centrifugations at 15,000 xg for 5 min, then for 15 min, both at 4ºC. A small
701 aliquot of the clear supernatant was taken for RNA quantification using the
702 Qubit RNA HS Assay Kit (Invitrogen, Q32852). The RNA concentration was
703 adjusted to 0.05 µg/µl with additional lysis buffer containing CHAPS, emetine,
704 and PIC. The supernatant was treated with RNase A (1 µg/ml) at 25ºC for 10
705 min to cleave unprotected RNA regions. After RNase treatment, 200 µl of
706 sample was applied to a 10-50% sucrose gradient prepared in polysome lysis
707 buffer and ultracentrifuged in a SW41Ti rotor at 30,000 xg for 3 h at 4ºC. After
708 centrifugation, gradients were fractionated from the top using a piston gradient
709 fractionator (BioComp, Canada).

710

Competing Interest Statement

The authors declare that the research was conducted in the absence of any commercial or financial relationships that could be construed as a potential conflict of interest.

Acknowledgments

We thank Dr Valérie Heurgué-Hamard (IBPC, Paris) and Dr. Bergmann (UMASS Medical School, Massachusetts) for generous gifts of antibody against methyl-eRF1 and UASp-P35 transgenic fly line, respectively. We acknowledge Bloomington Drosophila Stock Centre and Kyoto Stock Center for the fly stocks. Confocal images and Western blotting data were acquired with LSM900 and ChemiDoc Touch, respectively, at FBS Core Facility in Osaka University. Assistance with sucrose gradient analysis was provided by the Center for Medical Research and Education, Graduate School of Medicine, Osaka University. We appreciate the insightful discussion and suggestions from all the members of KT's laboratory.

Author Contributions

All authors contributed to the experiment design. XF, SR, KS, and KT performed all experiments. XF, SR and KS performed the computational analyses. XF, SR, KS, and KT wrote the paper. KS, IT, and KT supervised the project.

734 ## References

735 Avilés-Pagán, E.E., Orr-Weaver, T.L., 2018. Activating embryonic
736 development in *Drosophila*. Semin. Cell Dev. Biol. 84, 100–110.
737 Becker, T., Armache, J.-P., Jarasch, A., Anger, A.M., Villa, E., Sieber, H.,
738 Motaal, B.A., Mielke, T., Berninghausen, O., Beckmann, R., 2011.
739 Structure of the no-go mRNA decay complex Dom34–Hbs1 bound to a
740 stalled 80S ribosome. Nat. Struct. Mol. Biol. 18, 715–720.
741 Brandman, O., Hegde, R.S., 2016. Ribosome-associated protein quality
742 control. Nat. Struct. Mol. Biol. 23, 7–15.
743 Chen, C.-C., Wang, K.-Y., Shen, C.-K.J., 2013. DNA 5-methylcytosine
744 demethylation activities of the mammalian DNA methyltransferases. J.
745 Biol. Chem. 288, 9084–9091.
746 Chen, S., Zhou, Y., Chen, Y., Gu, J., 2018. fastp: an ultra-fast all-in-one
747 FASTQ preprocessor. Bioinformatics 34, i884–i890.
748 Clarke, S.G., 2013. Protein methylation at the surface and buried deep:
749 thinking outside the histone box. Trends Biochem. Sci. 38, 243–252.
750 Dai, X., Ren, T., Zhang, Y., Nan, N., 2021. Methylation multiplicity and its
751 clinical values in cancer. Expert Rev. Mol. Med. 23, e2.
752 Dej, K.J., Spradling, A.C., 1999. The endocycle controls nurse cell polytene
753 chromosome structure during *Drosophila* oogenesis. Development 126,
754 293–303.
755 Deng, W.-M., Althauser, C., Ruohola-Baker, H., 2001. Notch-Delta signaling
756 induces a transition from mitotic cell cycle to endocycle in *Drosophila*
757 follicle cells. Development 128, 4737–4746.
758 Dinçbas-Renqvist, V., Engström, Å., Mora, L., Heurgué-Hamard, V.,

759 Buckingham, R., Ehrenberg, M., 2000. A post-translational modification
760 in the GGQ motif of RF2 from Escherichia coli stimulates termination of
761 translation. EMBO J. 19, 6900–6907.
762 Dobin, A., Davis, C.A., Schlesinger, F., Drenkow, J., Zaleski, C., Jha, S.,
763 Batut, P., Chaisson, M., Gingeras, T.R., 2013. STAR: ultrafast
764 universal RNA-seq aligner. Bioinformatics 29, 15–21.
765 Doma, M.K., Parker, R., 2006. Endonucleolytic cleavage of eukaryotic
766 mRNAs with stalls in translation elongation. Nature 440, 561–564.
767 D'Orazio, K.N., Wu, C.C.-C., Sinha, N., Loll-Krippleber, R., Brown, G.W.,
768 Green, R., 2019. The endonuclease Cue2 cleaves mRNAs at stalled
769 ribosomes during No Go Decay. eLife 8, e49117.
770 Drummond-Barbosa, D., Spradling, A.C., 2001. Stem cells and their progeny
771 respond to nutritional changes during *Drosophila* oogenesis. Dev. Biol.
772 231, 265–278.
773 Fang, Q., Kimura, Y., Shimazu, T., Suzuki, T., Yamada, A., Dohmae, N.,
774 Iwasaki, S., Shinkai, Y., 2022. Mammalian HEMK1 methylates
775 glutamine residue of the GGQ motif of mitochondrial release factors.
776 Sci. Rep. 12, 4104.
777 Figaro, S., Scrima, N., Buckingham, R.H., Heurgué-Hamard, V., 2008.
778 HemK2 protein, encoded on human chromosome 21, methylates
779 translation termination factor eRF1. FEBS Lett. 582, 2352–2356.
780 Fuchs, Y., Steller, H., 2015. Live to die another way: modes of programmed
781 cell death and the signals emanating from dying cells. Nat. Rev. Mol.
782 Cell Biol. 16, 329–344.
783 Gao, J., Wang, B., Yu, H., Wu, G., Wan, C., Liu, W., Liao, S., Cheng, L., Zhu,

784 Z., 2020. Structural insight into HEMK2–TRMT112-mediated glutamine
785 methylation. Biochem. J. 477, 3833–3838.
786 Gates, L.A., Foulds, C.E., O'Malley, B.W., 2017. Histone marks in the 'Driver's
787 Seat': Functional roles in steering the transcription cycle. Trends
788 Biochem. Sci. 42, 977–989.
789 Gleason, R.J., Anand, A., Kai, T., Chen, X., 2018. Protecting and diversifying
790 the germline. Genetics 208, 435–471.
791 Glover, M.L., Burroughs, A.Max., Monem, P.C., Egelhofer, T.A., Pule, M.N.,
792 Aravind, L., Arribere, J.A., 2020. NONU-1 Encodes a conserved
793 endonuclease required for mRNA translation surveillance. Cell Rep.
794 30, 4321-4331.e4.
795 Goodrich, J.S., Clouse, K.N., Schüpbach, T., 2004. Hrb27C, Sqd and Otu
796 cooperatively regulate *gurken* RNA localization and mediate nurse cell
797 chromosome dispersion in *Drosophila* oogenesis. Development 131,
798 1949–1958.
799 Grieder, N.C., Cuevas, M.D., Spradling, A.C., 2000. The fusome organizes
800 the microtubule network during oocyte differentiation in *Drosophila*.
801 Development 127, 4253–4264.
802 Hayashi, S., Ito, K., Sado, Y., Taniguchi, M., Akimoto, A., Takeuchi, H.,
803 Aigaki, T., Matsuzaki, F., Nakagoshi, H., Tanimura, T., et al., 2002.
804 GETDB, a database compiling expression patterns and molecular
805 locations of a collection of gal4 enhancer traps. genesis 34, 58–61.
806 Heurgué-Hamard, V., Champ, S., Engström, A., Ehrenberg, M., Buckingham,
807 R.H., 2002. The hemK gene in *Escherichia coli* encodes the N(5)-
808 glutamine methyltransferase that modifies peptide release factors.

809 EMBO J. 21, 769–778.
810 Heurgué-Hamard, V., Champ, S., Mora, L., Merkoulova-Rainon, T., Kisselev,
811 L.L., Buckingham, R.H., 2005. The glutamine residue of the conserved
812 GGQ motif in *Saccharomyces cerevisiae* release factor eRF1 is
813 methylated by the product of the YDR140w gene. J. Biol. Chem. 280,
814 2439–2445.
815 Heurgué-Hamard, V., Graille, M., Scrima, N., Ulryck, N., Champ, S., van
816 Tilbeurgh, H., Buckingham, R.H., 2006. The zinc finger protein
817 Ynr046w is plurifunctional and a component of the eRF1
818 methyltransferase in yeast. J. Biol. Chem. 281, 36140–36148.
819 Ikeuchi, K., Izawa, T., Inada, T., 2019. Recent progress on the molecular
820 mechanism of quality controls induced by ribosome stalling. Front.
821 Genet. 9, 743.
822 Ishizawa, T., Nozaki, Y., Ueda, T., Takeuchi, N., 2008. The human
823 mitochondrial translation release factor HMRF1L is methylated in the
824 GGQ motif by the methyltransferase HMPrmC. Biochem. Biophys. Res.
825 Commun. 373, 99–103.
826 Jamar, N.H., Kritsiligkou, P., Grant, C.M., 2017. The non-stop decay mRNA
827 surveillance pathway is required for oxidative stress tolerance. Nucleic
828 Acids Res. 45, 6881–6893.
829 Jevitt, A., Chatterjee, D., Xie, G., Wang, X.-F., Otwell, T., Huang, Y.-C., Deng,
830 W.-M., 2020. A single-cell atlas of adult *Drosophila* ovary identifies
831 transcriptional programs and somatic cell lineage regulating oogenesis.
832 PLOS Biol. 18, e3000538.
833 Klotz, A.V., Thomas, B.A., Glazer, A.N., Blacher, R.W., 1990. Detection of

834 methylated asparagine and glutamine residues in polypeptides. Anal.
835 Biochem. 186, 95–100.
836 Klusza, S., Novak, A., Figueroa, S., Palmer, W., Deng, W.-M., 2013. Prp22
837 and spliceosome components regulate chromatin dynamics in germ-
838 line polyploid cells. PLoS ONE 8, e79048.
839 Kobayashi, K., Kikuno, I., Kuroha, K., Saito, K., Ito, K., Ishitani, R., Inada, T.,
840 Nureki, O., 2010. Structural basis for mRNA surveillance by archaeal
841 Pelota and GTP-bound EF1α complex. Proc. Natl. Acad. Sci. U. S. A.
842 107, 17575–17579.
843 Koch, R., Ledermann, R., Urwyler, O., Heller, M., Suter, B., 2009. Systematic
844 functional analysis of bicaudal-D serine phosphorylation and intragenic
845 suppression of a female sterile allele of BicD. PLoS ONE 4, e4552.
846 Kusevic, D., Kudithipudi, S., Jeltsch, A., 2016. Substrate specificity of the
847 HEMK2 protein glutamine methyltransferase and identification of novel
848 substrates. J. Biol. Chem. 291, 6124–6133.
849 Kweon, S.-M., Chen, Y., Moon, E., Kvederaviciutė, K., Klimasauskas, S.,
850 Feldman, D.E., 2019. An adversarial DNA N6-methyladenine-sensor
851 network preserves polycomb silencing. Mol. Cell 74, 1138-1147.e6.
852 Lacoux, C., Wacheul, L., Saraf, K., Pythoud, N., Huvelle, E., Figaro, S.,
853 Graille, M., Carapito, C., Lafontaine, D.L.J., Heurgué-Hamard, V.,
854 2020. The catalytic activity of the translation termination factor
855 methyltransferase Mtq2-Trm112 complex is required for large
856 ribosomal subunit biogenesis. Nucleic Acids Res. 48, 12310–12325.
857 Lasko, P., 2012. mRNA Localization and translational control in *Drosophila*
858 oogenesis. Cold Spring Harb. Perspect. Biol. 4, a012294.

859 Liao, Y., Smyth, G.K., Shi, W., 2014. featureCounts: an efficient general
860 purpose program for assigning sequence reads to genomic features.
861 Bioinformatics 30, 923–930.
862 Lim, L.-X., Isshiki, W., Iki, T., Kawaguchi, S., Kai, T., 2022. The tudor domain-
863 containing protein, Kotsubu (CG9925), localizes to the nuage and
864 functions in piRNA biogenesis in *D. melanogaster*. Front. Mol. Biosci.
865 9, 818302.
866 Liu, P., Nie, S., Li, B., Yang, Z.-Q., Xu, Z.-M., Fei, J., Lin, C., Zeng, R., Xu, G.-
867 L., 2010. Deficiency in a glutamine-specific methyltransferase for
868 release factor causes mouse embryonic lethality. Mol. Cell. Biol. 30,
869 4245–4253.
870 Love, M.I., Huber, W., Anders, S., 2014. Moderated estimation of fold change
871 and dispersion for RNA-seq data with DESeq2. Genome Biol. 15, 550.
872 McCall, K., 2004. Eggs over easy: cell death in the *Drosophila* ovary. Dev.
873 Biol. 274, 3–14.
874 Metzger, E., Wang, S., Urban, S., Willmann, D., Schmidt, A., Offermann, A.,
875 Allen, A., Sum, M., Obier, N., Cottard, F., et al. 2019. KMT9
876 monomethylates histone H4 lysine 12 and controls proliferation of
877 prostate cancer cells. Nat. Struct. Mol. Biol. 26, 361–371.
878 Patil, V.S., Kai, T., 2010. Repression of retroelements in *Drosophila* germline
879 via piRNA pathway by the tudor domain protein tejas. Curr. Biol. 20,
880 724–730.
881 Perkins, L.A., Holderbaum, L., Tao, R., Hu, Y., Sopko, R., McCall, K., Yang-
882 Zhou, D., Flockhart, I., Binari, R., Shim, H.-S., et al. 2015. The
883 transgenic RNAi project at Harvard medical school: Resources and

884 validation. Genetics 201, 843–852.
885 Pierson, W.E., Hoffer, E.D., Keedy, H.E., Simms, C.L., Dunham, C.M., Zaher,
886 H.S., 2016. Uniformity of peptide release Is maintained by methylation
887 of release factors. Cell Rep. 17, 11–18.
888 Ping, X.-L., Sun, B.-F., Wang, L., Xiao, W., Yang, X., Wang, W.-J., Adhikari,
889 S., Shi, Y., Lv, Y., Chen, Y.-S., et al. 2014. Mammalian WTAP is a
890 regulatory subunit of the RNA N6-methyladenosine methyltransferase.
891 Cell Res. 24, 177–189.
892 Polevoda, B., Span, L., Sherman, F., 2006. The Yeast translation release
893 factors Mrf1p and Sup45p (eRF1) are methylated, respectively, by the
894 methyltransferases Mtq1p and Mtq2p. J. Biol. Chem. 281, 2562–2571.
895 Ramazi, S., Zahiri, J., 2021. Post-translational modifications in proteins:
896 resources, tools and prediction methods. Database 2021, baab012.
897 Rastegari, E., Kajal, K., Tan, B.-S., Huang, F., Chen, R.-H., Hsieh, T.-S., Hsu,
898 H.-J., 2020. WD40 protein Wuho controls germline homeostasis via
899 TRIM-NHL tumor suppressor Mei-p26 in *Drosophila*. Development 147,
900 dev182063.
901 Ratel, D., Ravanat, J.-L., Charles, M.-P., Platet, N., Breuillaud, L., Lunardi, J.,
902 Berger, F., Wion, D., 2006. Undetectable levels of N6-methyl adenine
903 in mouse DNA: Cloning and analysis of PRED28, a gene coding for a
904 putative mammalian DNA adenine methyltransferase. FEBS Lett. 580,
905 3179–3184.
906 Ryšlavá, H., Doubnerová, V., Kavan, D., Vaněk, O., 2013. Effect of
907 posttranslational modifications on enzyme function and assembly. J.
908 Proteomics 92, 80–109.

909 Schaeffer, V., Althauser, C., Shcherbata, H.R., Deng, W.-M., Ruohola-Baker,
910 H., 2004. Notch-dependent Fizzy-Related/Hec1/Cdh1 expression is
911 required for the mitotic-to-endocycle transition in *Drosophila* follicle
912 cells. Curr. Biol. 14, 630–636.
913 Schindelin, J., Arganda-Carreras, I., Frise, E., Kaynig, V., Longair, M.,
914 Pietzsch, T., Preibisch, S., Rueden, C., Saalfeld, S., Schmid, B., et al.
915 2012. Fiji - an open source platform for biological image analysis. Nat.
916 Methods 9, 10.1038/nmeth.2019.
917 Shen, Y., Liu, W., Zuo, J., Han, J., Zhang, Z.C., 2021. Protocol for visualizing
918 newly synthesized proteins in primary mouse hepatocytes. STAR
919 Protoc. 2, 100616.
920 Simms, C.L., Yan, L.L., Zaher, H.S., 2017. Ribosome collision is critical for
921 quality control during no-go decay. Mol. Cell 68, 361-373.e5.
922 Sprung, R., Chen, Y., Zhang, K., Cheng, D., Zhang, T., Peng, J., Zhao, Y.,
923 2008. Identification and validation of eukaryotic aspartate and
924 glutamate methylation in proteins. J. Proteome Res. 7, 1001–1006.
925 St. Johnston, H.L.-S. and D., 2001. Delta signaling from the germ line controls
926 the proliferation and differentiation of the somatic follicle cells during
927 Drosophila oogenesis. Genes Dev. 15, 1393–1405.
928 Svidritskiy, E., Korostelev, A.A., 2018. Conformational control of translation
929 termination on the 70S ribosome. Structure 26, 821-828.e3.
930 Tan, K., Stupack, D.G., Wilkinson, M.F., 2022. Nonsense-mediated RNA
931 decay: an emerging modulator of malignancy. Nat. Rev. Cancer 22,
932 437–451.
933 Thomas, P.D., Ebert, D., Muruganujan, A., Mushayahama, T., Albou, L.-P.,

934 Mi, H., 2022. PANTHER: Making genome-scale phylogenetics
935 accessible to all. Protein Sci. 31, 8–22.
936 Tomomatsu S., Watanabe A., Tesina P., Hashimoto S., Ikeuchi K., Li S.,
937 Matsuo Y., Beckmann R., Inada T., 2023. Two modes of Cue2-
938 mediated mRNA cleavage with distinct substrate recognition initiate no-
939 go decay. Nucleic Acids Res. 51, 253–270.
940 Tsuboi, T., Kuroha, K., Kudo, K., Makino, S., Inoue, E., Kashima, I., Inada, T.,
941 2012. Dom34:Hbs1 plays a general role in quality-control systems by
942 dissociation of a stalled ribosome at the 3′ end of aberrant mRNA. Mol.
943 Cell 46, 518–529.
944 Wall, A.A., Phillips, A.M., Kelly, L.E., 2005. Effective translation of the second
945 cistron in two *Drosophila* dicistronic transcripts is determined by the
946 absence of In-frame AUG codons in the first cistron. J. Biol. Chem.
947 280, 27670–27678.
948 Wang, X., Feng, J., Xue, Y., Guan, Z., Zhang, D., Liu, Z., Gong, Z., Wang, Q.,
949 Huang, J., Tang, C., et al., 2016. Structural basis of N6-adenosine
950 methylation by the METTL3–METTL14 complex. Nature 534, 575–578.
951 Werz, C., Lee, T.V., Lee, P.L., Lackey, M., Bolduc, C., Stein, D.S., Bergmann,
952 A., 2005. Mis-specified cells die by an active gene-directed process,
953 and inhibition of this death results in cell fate transformation in
954 *Drosophila*. Development 132, 5343–5352.
955 Woodcock, C.B., Yu, D., Zhang, X., Cheng, X., 2019. Human
956 HemK2/KMT9/N6AMT1 is an active protein methyltransferase, but
957 does not act on DNA in vitro, in the presence of Trm112. Cell Discov.
958 5, 50.

959 Wu, C.C.-C., Peterson, A., Zinshteyn, B., Regot, S., Green, R., 2020.
960 Ribosome collisions trigger general stress responses to regulate cell
961 fate. Cell 182, 404-416.e14.
962 Xiao, C.-L., Zhu, S., He, M., Chen, D., Zhang, Q., Chen, Y., Yu, G., Liu, J.,
963 Xie, S.-Q., Luo, F., et al. 2018. N6-methyladenine DNA modification in
964 the human genome. Mol. Cell 71, 306-318.e7.
965 Zinoviev, A., Ayupov, R.K., Abaeva, I.S., Hellen, C.U.T., Pestova, T.V., 2020.
966 Extraction of mRNA from stalled ribosomes by the ski complex. Mol.
967 Cell 77 1340-1349.e6
968 Zhao, Y., Garcia, B.A., 2015. Comprehensive catalog of currently documented
969 histone modifications. Cold Spring Harb. Perspect. Biol. 7, a025064.
970
971

972 # Legends

973 **Figure 1: HemK2 is essential for *Drosophila* germline development**

974 (A) Diagrammatic illustration of *Drosophila* oogenesis. Each ovariole is composed of a
975 germarium at the anterior end, followed by progressively developing egg chambers. A
976 16-cell germline cyst enclosed with somatic follicle cells buds out of germarium,
977 forming an egg chamber. Of those 16 germline cells, one differentiates into the oocyte,
978 while others become nurse cells.

979 (B) Representative images of ovarian morphology from control and *hemK2* germline
980 knockdown (GLKD) samples. *hemK2*-GLKD leads to female sterility, characterized by
981 arrested development of egg chambers at stages 7-8 and impaired vitellogenesis.
982 Scale bar, 250 μm.

983 (C) Quantitative RT-PCR confirmation of knockdown efficacy in *hemK2*-GLKD ovaries.
984 Expression levels are normalized to *rp49* with *tubulin* serving as an internal control.
985 Standard deviation is denoted by error bars (n=3).

986 (D) Analysis of egg laying and hatching rate. Infertility observed in *hemK2*-GLKD is
987 rescued by expression of the wild-type FLAG-tagged HemK2 transgene using the
988 germline-specific driver *NGT40*; *nosGal4-VP16*. Daily egg production by 3 females
989 was recorded (n=3). Error bars represent standard deviation.

990 (E) Immunofluorescence of FLAG-tagged HemK2 (green) and DNA (DAPI, blue) in
991 ovaries of the indicated genotypes corresponding to (D). Arrows highlight degenerated
992 egg chambers in *hemK2*-GLKD and later-stage egg chambers following FLAG-HemK2

993 expression. Scale bars, 50 μm.

994 (F) Western blot analysis detecting FLAG epitope to demonstrate germline expression
995 of FLAG-HemK2 wildtype in ovarian extracts. Tubulin is utilized as a loading control.

996

997 **Figure 2: Knockdown of hemK2 leads pleiotropic defects in germline**
998 **development**

999 (A) Ovaries displaying mitotic marker phospho-histone H3 (pH3) (red) and DAPI (blue)
1000 (left panel). Dotted rectangles highlight hyperplastic posterior follicle cells in *hemK2*-
1001 GLKD (upper right panel). Scale bars, 20 μm. Quantification of ovarioles with single
1002 versus multi-layered follicle cells is provided (right panel, n=100).

1003 (B) Immunostaining for nucleolar marker Fibrillarin and DNA (DAPI) in stage 7/8 egg
1004 chambers. Insets show enlarged views of nurse cell nuclei with either dispersed or
1005 undispersed chromosomes. Scale bars, 10 μm.

1006 (C) Quantitative RT-PCR analysis of gene expression involved in chromosomal
1007 dispersion, with standard deviation indicated by error bars (n=3).

1008 (D) Immunostaining for apoptosis marker p53 and DNA (DAPI) in ovaries (left panel).
1009 Arrows indicate p53 signal accumulation in nurse cell nuclei. Scale bars, 20 μm.
1010 Percentage of ovarioles displaying p53 signals is quantified (right panel, n=100).

1011

1012 **Figure 3: HemK2 functions for eRF1 methylation in *Drosophila***

1013 (A) Immunoprecipitation of endogenous eRF1 and subsequent Western blot analysis
1014 for N5-methyl-glutamine (Methyl-Q) from ovarian lysates, indicating a significant
1015 reduction in eRF1 methylation in *hemK2*-GLKD compared to control ovaries (bottom
1016 panel). Quantification of methyl-Q band intensity normalized to eRF1 signal is shown
1017 (right panel), with error bars representing standard deviation (n=3) and *p*-value
1018 indicated (unpaired *t*-test).

1019 (B) Immunostaining of methylated eRF1 (green) and total eRF1 (red) in control and
1020 *hemK2*-GLKD ovaries. Arrows indicate the cytoplasm of germline cells. Scale bars, 20
1021 µm.

1022 (C) Immunoprecipitation of germline-expressed FLAG-tagged eRF1 from ovaries.
1023 Western blot for methyl-Q illustrates a notable decrease in methylation of FLAG-eRF1
1024 in *hemK2*-GLKD. Nonspecific bands are marked with asterisks. Right panel shows
1025 quantification of methyl-Q band intensity normalized to FLAG-eRF1, as in (A), with
1026 error bars denoting standard deviation (n=3) and *p*-value provided (unpaired *t*-test).

1027 (D) Immunoprecipitation of Myc-tagged eRF1 (WT or Q185A mutant) in S2 cells, with
1028 Western blot detection for methyl-Q. Quantifications of methyl-Q band intensities
1029 normalized to Myc-eRF1 are shown with error bars representing standard deviation
1030 (n=3).

1031

1032 **Figure 4: The conserved NPPY motif of HemK2 is critical for eRF1 methylation**

1033 (A) Illustration of the methyltransferase (MTase) domain within *Drosophila* HemK2,

1034 highlighting the highly conserved NPPY motif across various species. Asn116 and
1035 Tyr119 of *Drosophila* HemK2 are mutated to Ala, generating N116A and Y119A,
1036 respectively.

1037 (B) Crystal structure depiction of human HemK2-TRMT112 complexed with methyl-
1038 glutamine (Methyl-Q) and S-adenosylhomocysteine (SAH) (Gao et al., 2020), focusing
1039 on the active site proximal to methyl-Q. HemK2 is depicted in gray, methyl-Q in green
1040 with hydrogen bonds around the methyl-Q. N122 and Y125 of human HemK2
1041 correspond to N116 and Y119 in *Drosophila* HemK2, respectively.

1042 (C) Immunostaining for FLAG-tagged HemK2 variants against a DNA counterstain
1043 (DAPI) in ovaries of the respective genotypes. Perturbation of proper oogenesis in
1044 *hemK2*-GLKD ovaries is restored by the expression of the N116A HemK2 variant but
1045 not the Y119A. Scale bars, 50 μm.

1046 (D) Analysis of egg laying and hatching rate for each genotype as described in (C).
1047 The number of eggs were counted daily for groups of three females (n=3), with
1048 standard deviation shown as error bars.

1049 (E) Immunoprecipitation followed by Western blot analysis for methyl-Q in S2 cells.
1050 Co-transfection of FLAG-tagged HemK2 and Myc-tagged eRF1, with or without *hemK2*
1051 knockdown (KD), demonstrates that eRF1 methylation loss in *hemK2*-KD is restored
1052 by wildtype HemK2 and the N116A mutant but not by the Y119A mutant. The lower
1053 panel provides quantification of methyl-Q intensity relative to Myc-eRF1 with standard
1054 deviation (n=3).

1055

1056 **Figure 5: eRF1 methylation ensures proper progression of oogenesis and**

1057 **efficient translation**

1058 (A) Comparative morphological images of control and *eRF1* germline knockdown

1059 (*eRF1*-GLKD) ovaries. Scale bar, 250 μm.

1060 (B) Analysis of egg production and hatching rate across different genotypes. The

1061 numbers of the eggs were counted daily for groups of three females (n=3), with error

1062 bars representing standard deviation.

1063 (C) Immunostaining of wild-type and Q185A mutant FLAG-tagged eRF1 (green), with

1064 Vas (red) marking germline cells, and DAPI (blue) for DNA, in ovaries corresponding

1065 to each genotype listed in (B). Loss of germline cells by *eRF1*-GLKD is restored with

1066 wild-type eRF1 but not with the Q185A mutant. Scale bars, 20 μm.

1067 (D) Immunostaining for FLAG-tagged eRF1 Q185A (red) and DNA (DAPI, blue) in

1068 ovaries. Overexpression of FLAG-eRF1 Q185A in wild-type background recapitulates

1069 the phenotypic consequences of *hemK2*-GLKD. Arrows point to degenerating egg

1070 chambers. Insets show enlarged views of nurse cell nuclei. Scale bars, 50 μm.

1071 (E) Protein synthesis assay using L-homopropargylglycine (HPG) in ovaries for each

1072 genotype indicated (green in left panels), with concurrent immunostaining for FLAG-

1073 HemK2 (red). Scale bars, 20 μm. The right panel shows quantification of HPG signal

1074 intensity, with measurements from representative images (n=5) and standard deviation

1075 as error bars.

1076

1077 **Figure 6: Knockdown of *hemK2* leads mRNA reduction and ribosome stalling**

1078 (A) Gene Ontology (GO) analysis of genes downregulated in *hemK2*-GLKD ovaries.
1079 Enrichment of GO biological process terms is analyzed by PANTHER (version 18.0).
1080 The fold enrichments are plotted and colored by their False Discovery Rate (FDR)
1081 values.

1082 (B) GO analysis for genes upregulated in *hemK2*-GLKD ovaries, conducted similarly
1083 to panel (A).

1084 (C) Volcano plot representing the differential expression of germline-enriched genes
1085 in *hemK2*-GLKD ovaries, with significance threshold set at *p*-value < 0.05 and $\log_2$FC
1086 < -1 or >1 (orange). Gene classification is based on single-cell mRNA-seq analysis of
1087 *Drosophila* ovaries (Jevitt et al., 2020).

1088 (D) Log_2-fold changes of cell-type enriched genes in *hemK2*-GLKD ovaries relative to
1089 control, with mean values and standard deviation depicted.

1090 (E) Ribosome profiling in ovarian lysates from control (blue), *hemK2*-GLKD (red), and
1091 double-germline knockdown of *hemK2* and *ski8* (green). Monosome and disome were
1092 separated using sucrose gradient sedimentation. Absorbance at 254 nm was recorded
1093 to generate elution profiles, normalized to the monosome peak for each sample. Insets
1094 highlight the disome peaks.

1095 (F) Disome to monosome peak ratios were calculated across three experimental

1096 replicates. Bar graphs represent average ratios with standard deviation (n=3) and *p*-
1097 value (unpaired *t*-test).

1098

1099 **Figure 7: Blockage of No-Go-decay pathway restores oogenesis defects in**
1100 ***hemK2*-GLKD ovaries.**

1101 (A) Fluorescent staining with DAPI for DNA in ovaries from various genotypes. Rescue
1102 of the oogenesis defects observed in *hemK2*-GLKD is achieved through combined
1103 knockdown of *ski8* or *pelo*, but not with *CG7139* or *upf3*. Scale bars, 50 µm.

1104 (B) Analysis of egg production and hatching rate for the indicated genotypes. The
1105 numbers of egg counted for groups of three females each day (n=3), with error bars
1106 representing standard deviation.

1107 (C) Assay of protein synthesis in ovaries using L-homopropargylglycine (HPG), across
1108 the specified genotypes. Scale bars, 20 µm.

1109 (D) Quantitative analysis of HPG fluorescence intensity for each genotype, with
1110 measurements taken from representative images (n=5). Error bars denote standard
1111 deviation.

1112 (E) Box plot depicting the $\log_2$-fold changes of genes enriched in germline 2 cell type
1113 in ovaries from *hemK2*-GLKD, *ski8-hemK2* DGKD, and *pelo-hemK2* DGKD compared
1114 to control. Paired *t*-test *p*-values are presented, comparing *hemK2* single knockdown
1115 with each respective double knockdown.

Figure 1

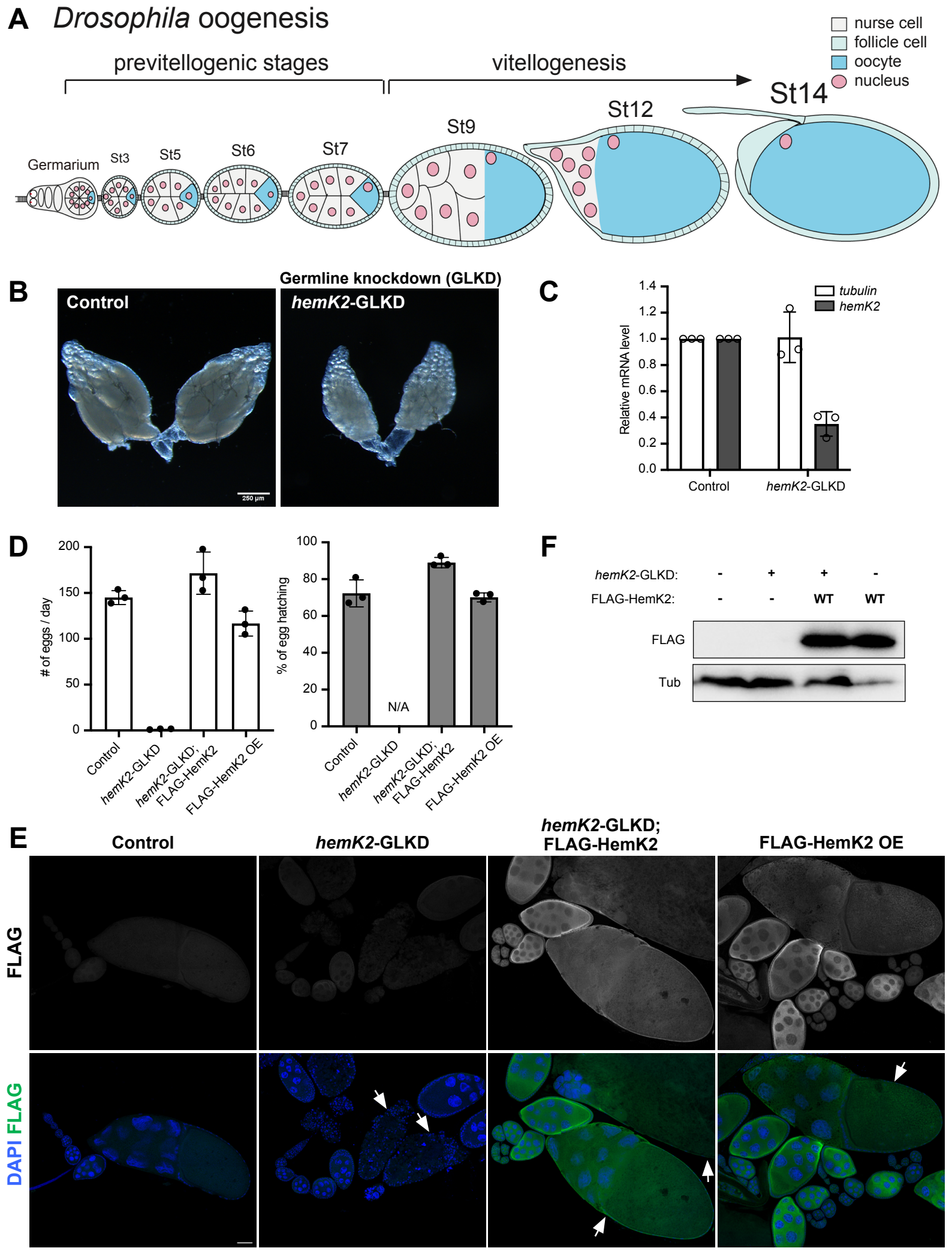
A
Drosophila oogenesis
nurse cell
follicle cell
oocyte
nucleus
previtellogenic stages
vitellogenesis
Germarium
St3
St5
St6
St7
St9
St12
St14
B
Germline knockdown (GLKD)
Control
hemK2-GLKD
250 µm
C
tubulin
hemK2
Relative mRNA level
1.4
1.2
1.0
0.8
0.6
0.4
0.2
0.0
Control
hemK2-GLKD
D
# of eggs / day
200
150
100
50
0
Control
hemK2-GLKD
hemK2-GLKD; FLAG-HemK2
FLAG-HemK2 OE
% of egg hatching
100
80
60
40
20
0
N/A
Control
hemK2-GLKD
hemK2-GLKD; FLAG-HemK2
FLAG-HemK2 OE
F
hemK2-GLKD: - + + -
FLAG-HemK2: - - WT WT
FLAG
Tub
E
Control
hemK2-GLKD
hemK2-GLKD; FLAG-HemK2
FLAG-HemK2 OE
FLAG
DAPI FLAG

Figure 2

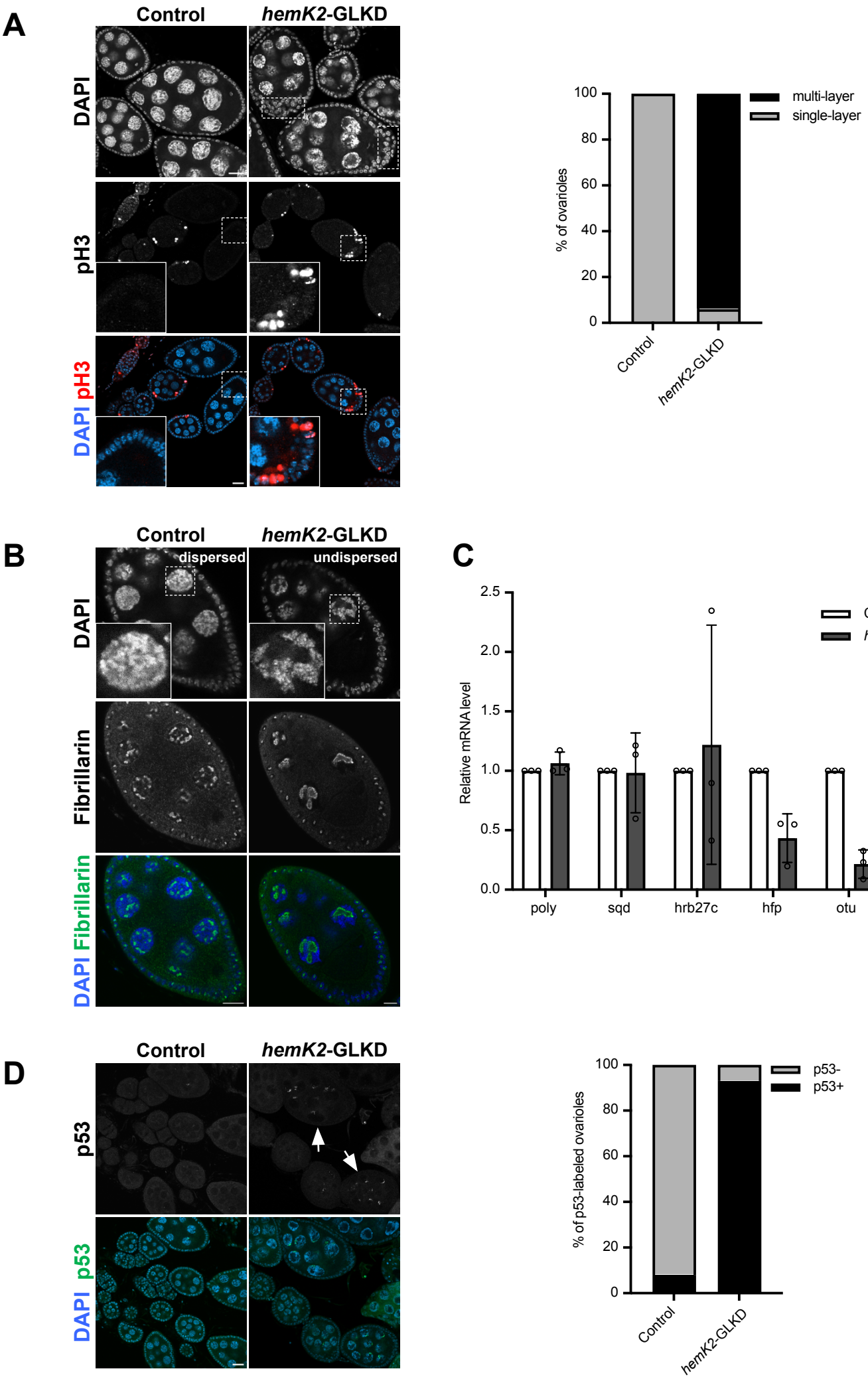
A
Control
hemK2-GLKD
DAPI
pH3
DAPI pH3
multi-layer
single-layer
% of ovarioles
100
80
60
40
20
0
Control
hemK2-GLKD
B
Control
hemK2-GLKD
dispersed
undispersed
DAPI
Fibrillarin
DAPI Fibrillarin
C
Control
hemK2-GLKD
Relative mRNA level
2.5
2.0
1.5
1.0
0.5
0.0
poly
sqd
hrb27c
hfp
otu
smn
D
Control
hemK2-GLKD
p53
DAPI p53
p53-
p53+
% of p53-labeled ovarioles
100
80
60
40
20
0
Control
hemK2-GLKD

Figure 3

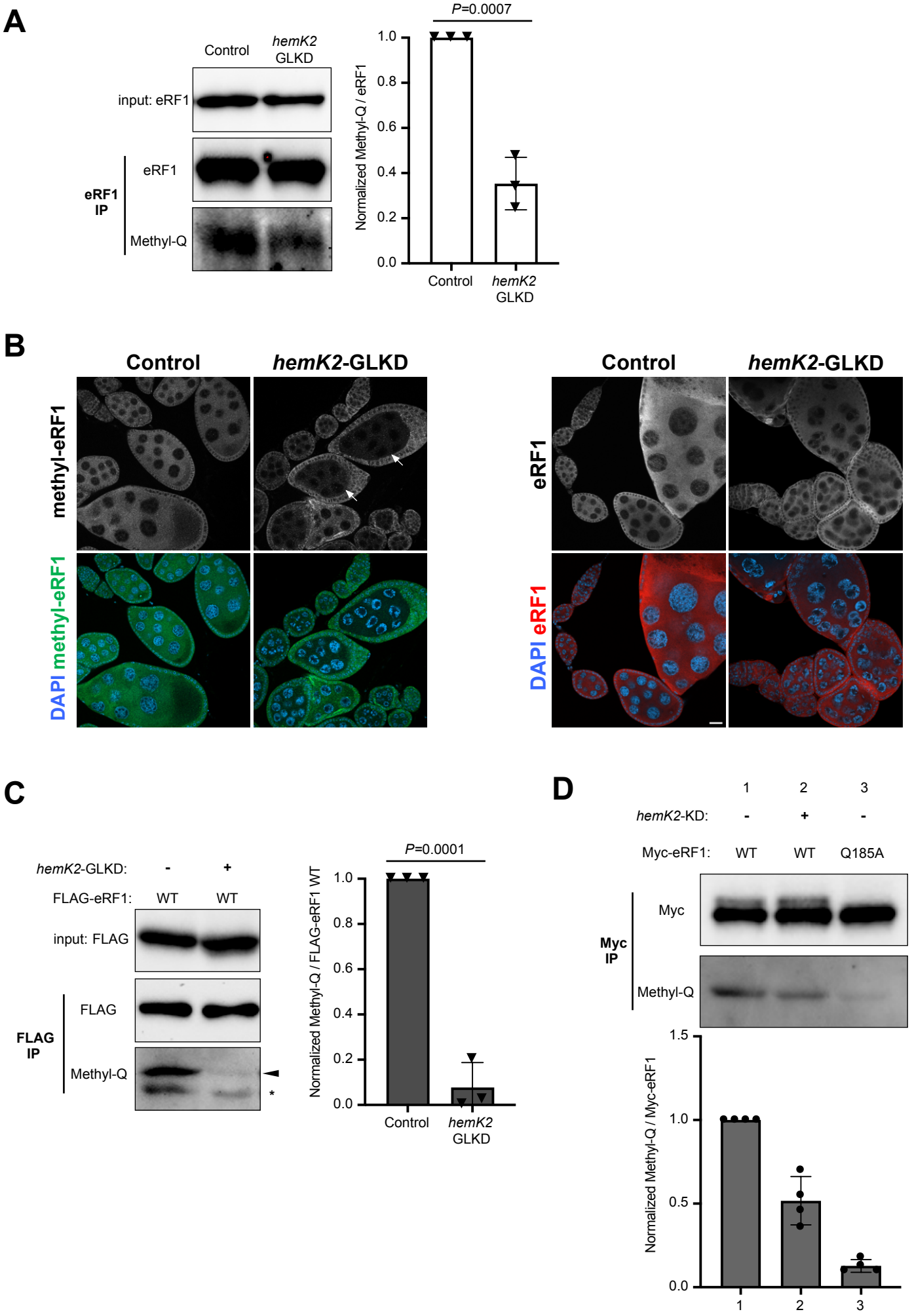
A
Control
hemK2 GLKD
input: eRF1
eRF1
eRF1 IP
Methyl-Q
P=0.0007
Normalized Methyl-Q / eRF1
1.0
0.8
0.6
0.4
0.2
0.0
Control
hemK2 GLKD
B
Control
hemK2-GLKD
methyl-eRF1
DAPI methyl-eRF1
Control
hemK2-GLKD
eRF1
DAPI eRF1
C
hemK2-GLKD: - +
FLAG-eRF1: WT WT
input: FLAG
FLAG
FLAG IP
Methyl-Q
P=0.0001
Normalized Methyl-Q / FLAG-eRF1 WT
1.0
0.8
0.6
0.4
0.2
0.0
Control
hemK2 GLKD
D
1 2 3
hemK2-KD: - + -
Myc-eRF1: WT WT Q185A
Myc
Myc IP
Methyl-Q
Normalized Methyl-Q / Myc-eRF1
1.5
1.0
0.5
0.0
1
2
3

Figure 4

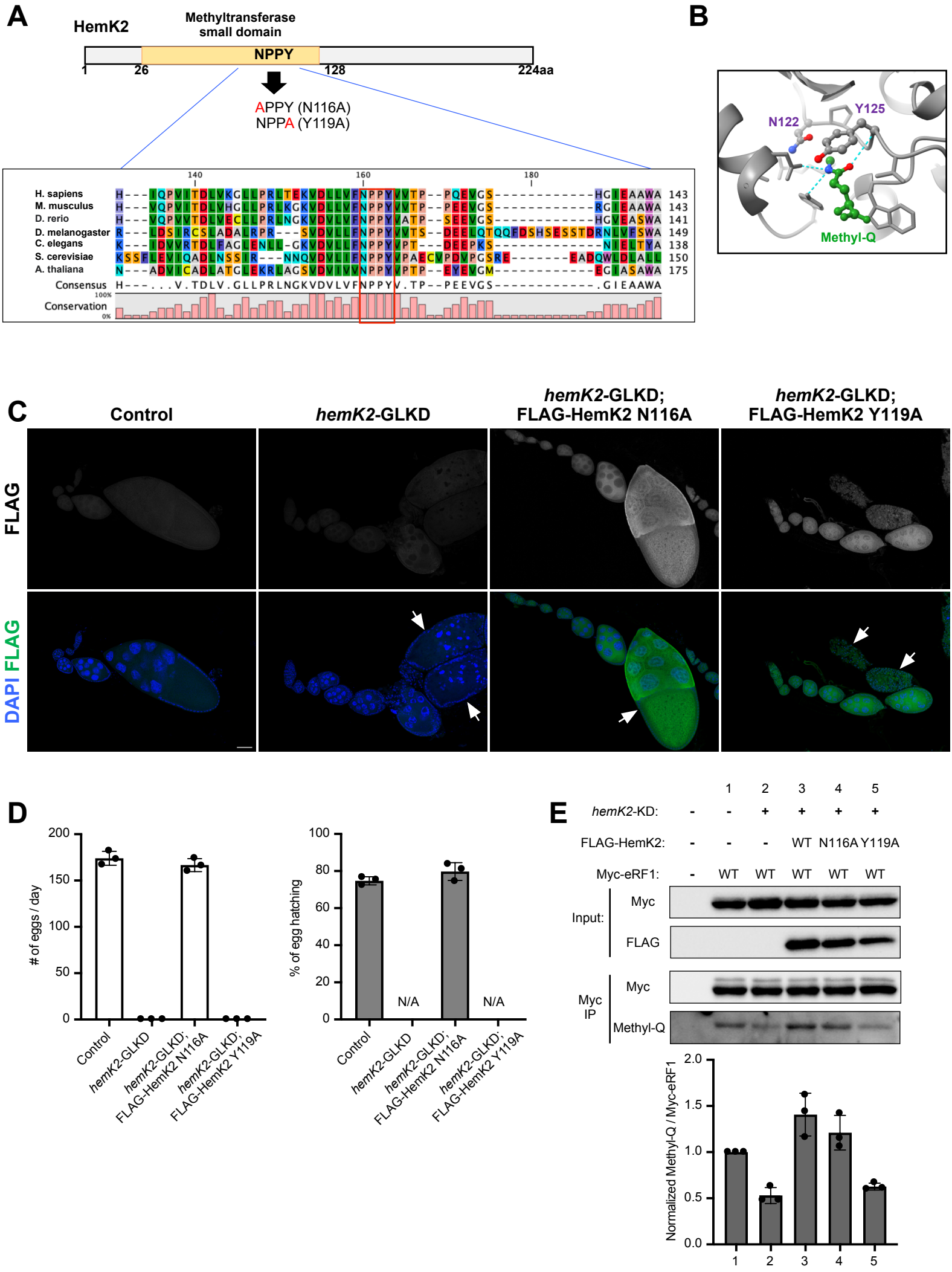
A
HemK2
Methyltransferase small domain
NPPY
1
26
128
224aa
APPY (N116A)
NPPA (Y119A)
H. sapiens
M. musculus
D. rerio
D. melanogaster
C. elegans
S. cerevisiae
A. thaliana
Consensus
Conservation
B
N122
Y125
Methyl-Q
C
Control
hemK2-GLKD
hemK2-GLKD; FLAG-HemK2 N116A
hemK2-GLKD; FLAG-HemK2 Y119A
FLAG
DAPI FLAG
D
# of eggs / day
% of egg hatching
N/A
N/A
Control
hemK2-GLKD
hemK2-GLKD; FLAG-HemK2 N116A
hemK2-GLKD; FLAG-HemK2 Y119A
E
hemK2-KD:
FLAG-HemK2:
Myc-eRF1:
WT
N116A
Y119A
Input:
Myc
FLAG
Myc IP
Methyl-Q
Normalized Methyl-Q / Myc-eRF1

Figure 5

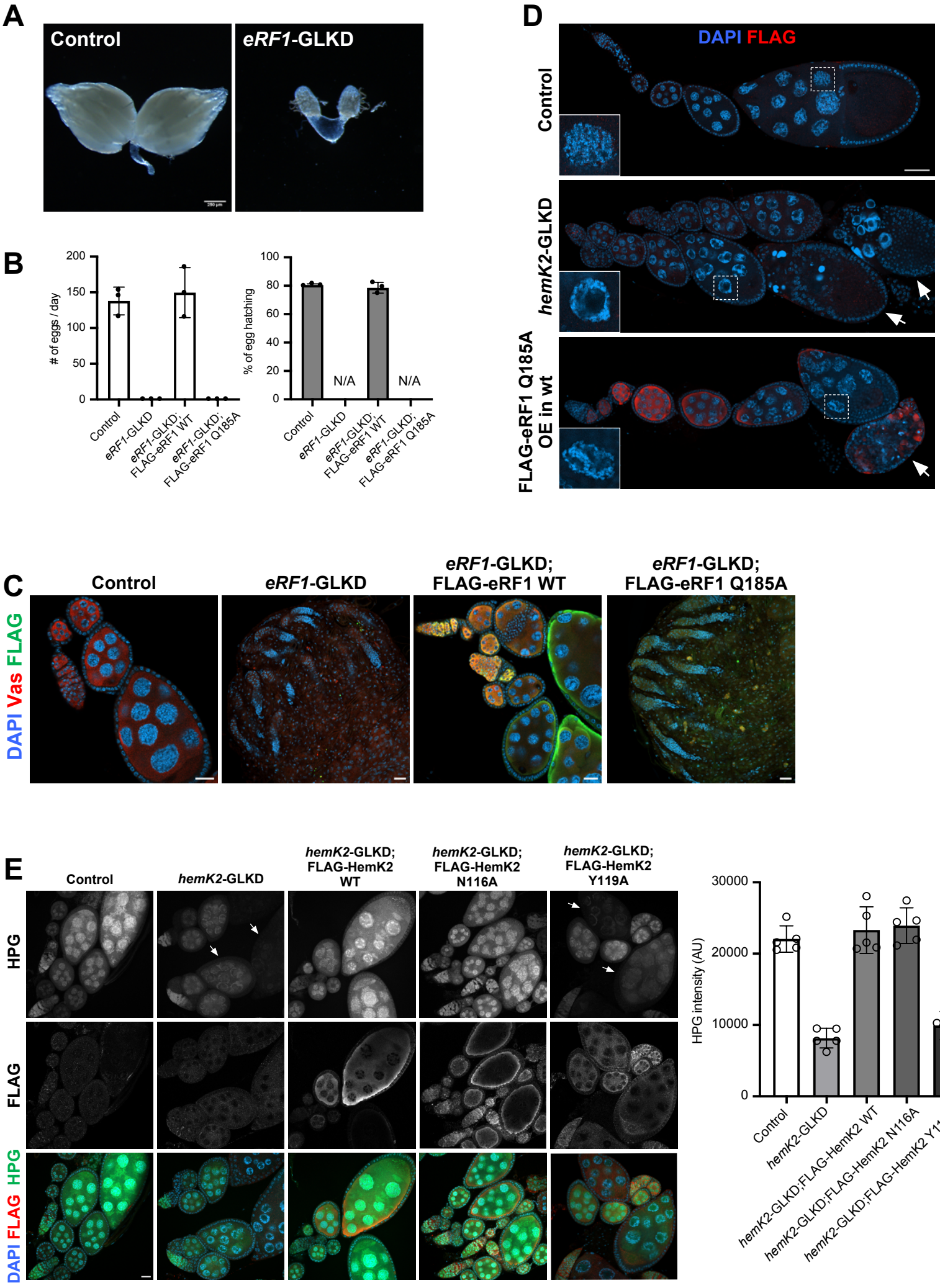
A
Control
eRF1-GLKD
B
# of eggs / day
200
150
100
50
0
Control
eRF1-GLKD
eRF1-GLKD; FLAG-eRF1 WT
eRF1-GLKD; FLAG-eRF1 Q185A
% of egg hatching
100
80
60
40
20
0
N/A
N/A
D
DAPI FLAG
Control
hemK2-GLKD
FLAG-eRF1 Q185A OE in wt
C
Control
eRF1-GLKD
eRF1-GLKD; FLAG-eRF1 WT
eRF1-GLKD; FLAG-eRF1 Q185A
DAPI Vas FLAG
E
Control
hemK2-GLKD
hemK2-GLKD; FLAG-HemK2 WT
hemK2-GLKD; FLAG-HemK2 N116A
hemK2-GLKD; FLAG-HemK2 Y119A
HPG
FLAG
DAPI FLAG HPG
HPG intensity (AU)
30000
20000
10000
0
Control
hemK2-GLKD
hemK2-GLKD;FLAG-HemK2 WT
hemK2-GLKD;FLAG-HemK2 N116A
hemK2-GLKD;FLAG-HemK2 Y119A

Figure 6

A

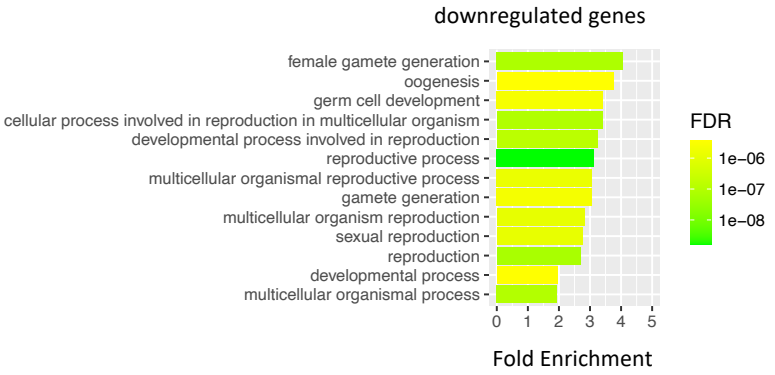

B

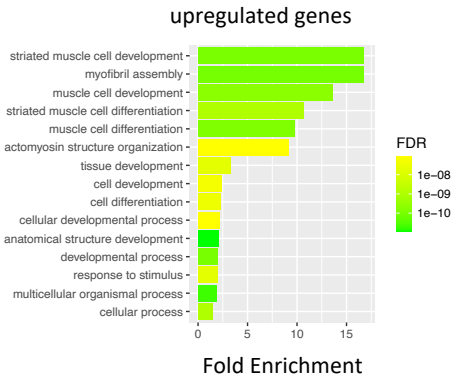

C

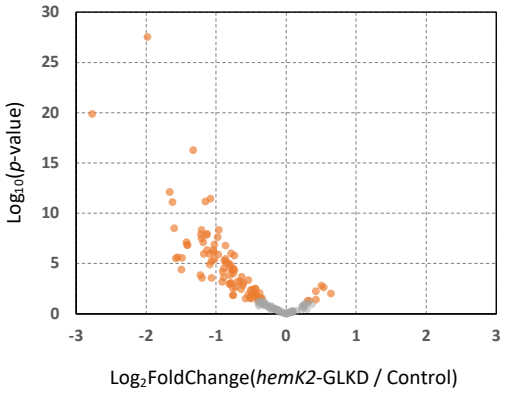

D

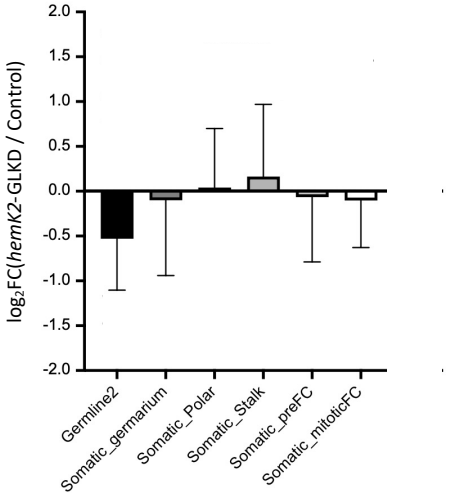

E

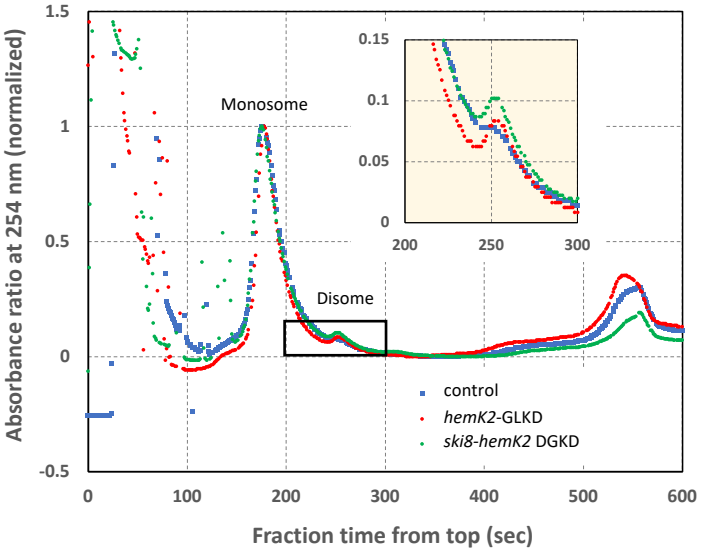

F

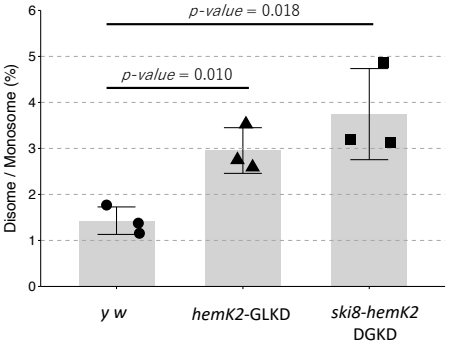

Figure 7

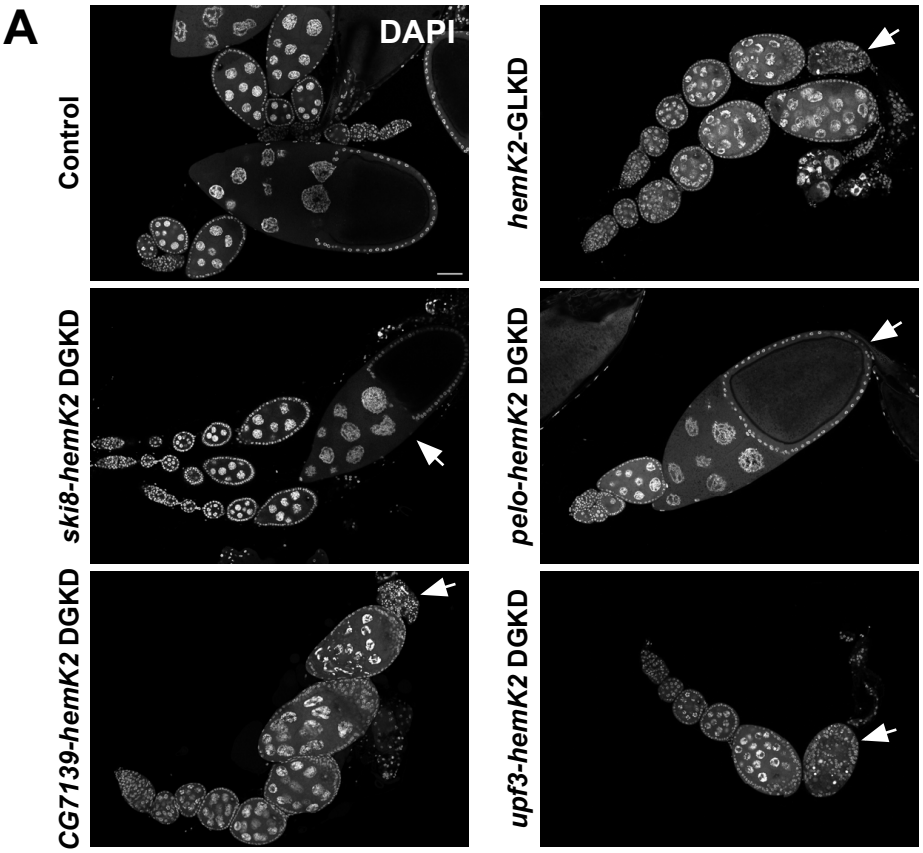
A
DAPI
Control
hemK2-GLKD
ski8-hemK2 DGKD
pelo-hemK2 DGKD
CG7139-hemK2 DGKD
upf3-hemK2 DGKD

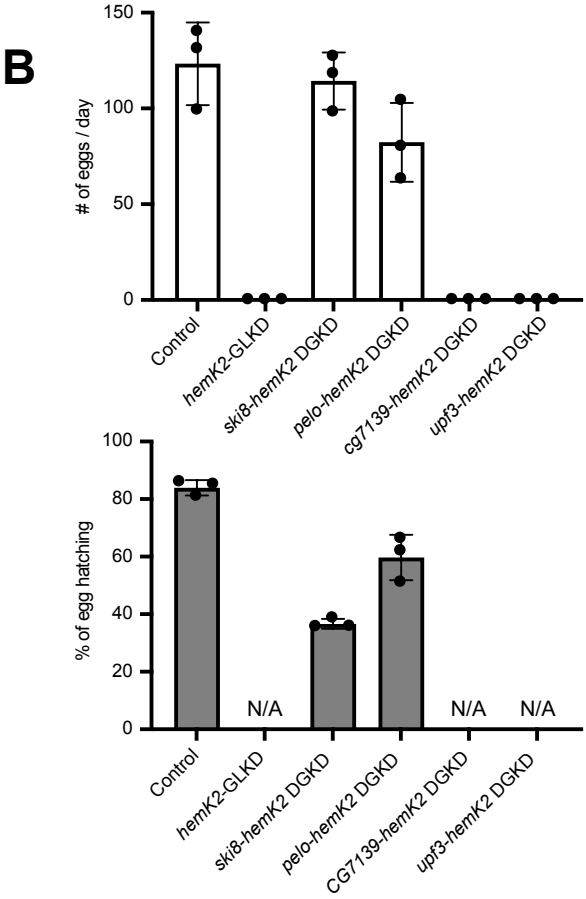
B
# of eggs / day
150
100
50
0
Control
hemK2-GLKD
ski8-hemK2 DGKD
pelo-hemK2 DGKD
cg7139-hemK2 DGKD
upf3-hemK2 DGKD
% of egg hatching
100
80
60
40
20
0
N/A
N/A
N/A
Control
hemK2-GLKD
ski8-hemK2 DGKD
pelo-hemK2 DGKD
CG7139-hemK2 DGKD
upf3-hemK2 DGKD

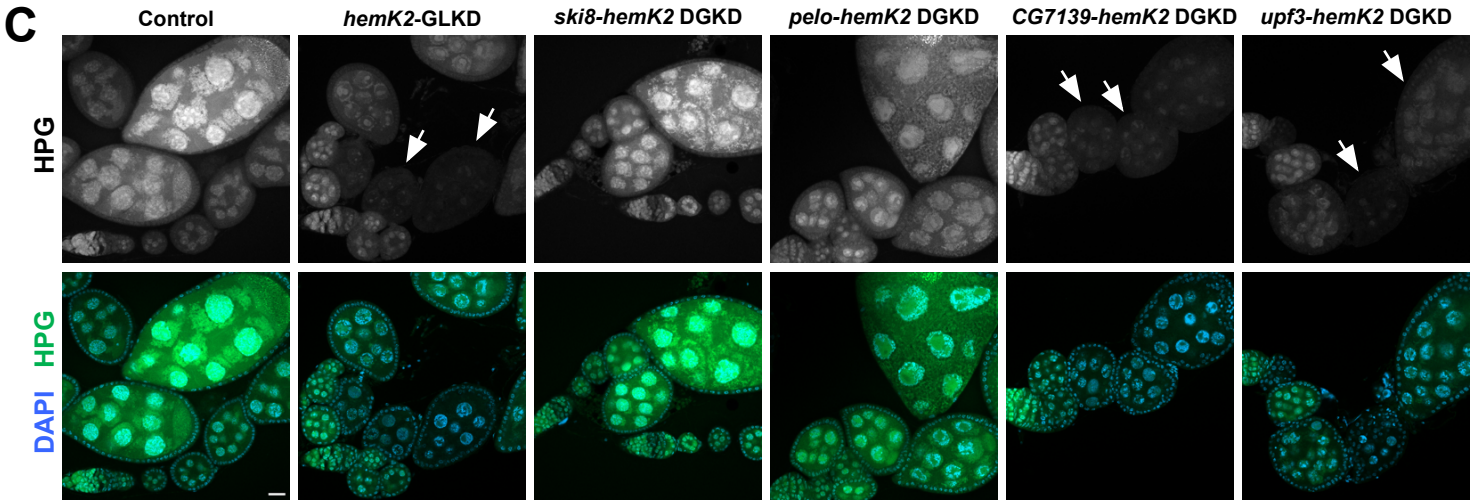
C
Control
hemK2-GLKD
ski8-hemK2 DGKD
pelo-hemK2 DGKD
CG7139-hemK2 DGKD
upf3-hemK2 DGKD
HPG
DAPI HPG

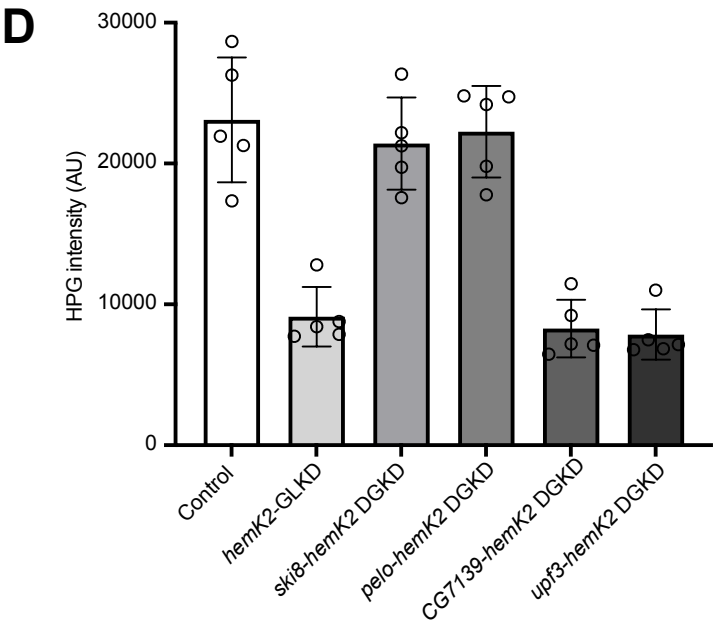
D
HPG intensity (AU)
30000
20000
10000
0
Control
hemK2-GLKD
ski8-hemK2 DGKD
pelo-hemK2 DGKD
CG7139-hemK2 DGKD
upf3-hemK2 DGKD

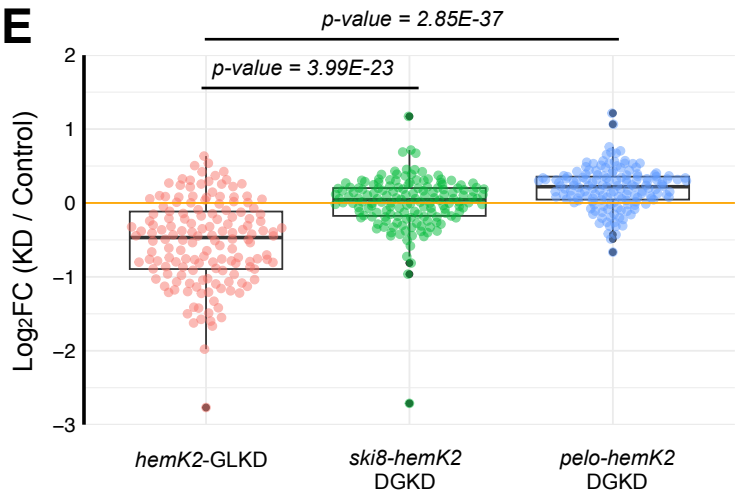
E
p-value = 2.85E-37
p-value = 3.99E-23
Log2FC (KD / Control)
2
1
0
−1
−2
−3
hemK2-GLKD
ski8-hemK2 DGKD
pelo-hemK2 DGKD